



**Hochschule Karlsruhe**  
University of Applied Sciences

## BACHELOR THESIS

**Cédric Uden**

**Exploring implementations for online control & optimisation  
applications in the operation of a particle accelerator**



**CERN**

Conseil Européen pour la Recherche Nucléaire  
1211 Geneva 23, Switzerland

Professional Supervisor	Dr. Alexander Huschauer
First Academic Supervisor	Prof. Dr.-Ing. Laubenheimer
Second Academic Supervisor	Prof. Dr. Nochta

03 February 2023





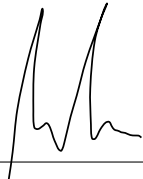
## **Affidavit**

I hereby assert under oath, that I completed the bachelor thesis in hand autonomously and that I used only those references mentioned in the appendix.

## **Eidesstattliche Erklärung**

Ich versichere hiermit eidesstattlich, dass ich die vorliegende Bachelor–Thesis selbstständig erarbeitet und dabei keine anderen als die angegebenen Quellen verwendet habe.

Date 03 February 2023

Signature  \_\_\_\_\_



# Abstract

This bachelor thesis has been conducted at the European Organization for Nuclear Research (CERN) in the framework of the technical student programme. The focus of this work was the implementation of a control and optimisation algorithm to counteract a recurring drift in a specific process in a particle accelerator: the CERN Proton Synchrotron. The goal was to increase the overall efficiency of said process by achieving an increase in performance and increase in autonomy.

The work presented in this thesis covers the following domains: learning the fundamentals in accelerator physics to understand the problem at hand, incorporating the computational infrastructure at CERN to implement a solution and studying certain control and optimisation algorithms to leverage their capabilities.

Subsequently, the technicalities of the general setup will be clarified before explaining the design of the cost function for the algorithm. As the performance of this specific process is influenced by different factors, the cost function must cover multiple objectives simultaneously. The complexity induced by the different features of the cost function as well as the methodology adopted for testing were studied in detail.

In the final observations the achievements reached in this study are highlighted and the caveats are summarised. The observations were based on findings made in large categorical time series that are difficult to process. A specialised tool is presented, which was developed specifically for this task and greatly facilitated the analysis of the time series.

Finally, an outlook is given based on the discoveries made in this study and the next actions in this project will be presented. Additionally, possibilities to improve the cost function in the future thanks to planned hardware upgrades are discussed.



# Zusammenfassung

Diese Bachelorarbeit wurde an der Europäischen Organisation für Kernforschung (CERN) im Rahmen des Technical Student Programms durchgeführt. Der Fokus der Thesis liegt in der Anwendung eines Kontroll- und Optimierungsalgorithmus, um einer wiederkehrenden langsamen Abwanderung eines speziellen Prozesses in einem Teilchenbeschleuniger, dem CERN Proton Synchrotron, entgegenzuwirken. Das Ziel war es, dessen Effizienz zu steigern, indem eine bessere Leistung und höhere Autonomie erzielt wurde.

Die Arbeit setzt Wissen in den gewissen Domänen voraus, welche dementsprechend im Laufe der Arbeit präsentiert werden: die Grundlagen der Beschleunigerphysik, um das Problem zu verstehen, die Computerinfrastruktur am CERN, um eine Lösung zu implementieren und das Verstehen von bestimmten Kontroll- und Optimierungsalgorithmen, um deren Fähigkeiten wirksam einzusetzen.

Nachdem anschließend die Rahmenbedingungen erklärt werden, wird der Entwurf der Kostenfunktion für den Algorithmus präsentiert. Da die Leistung dieses bestimmten Prozesses von mehreren Faktoren abhängig ist, muss die Entwicklung der Kostenfunktion mehrere Ziele gleichzeitig verfolgen. Die Komplexität durch diese Voraussetzung der Kostenfunktion und die genutzte Methodologie um diese effizient zu testen wurden detailliert analysiert.

Nachdem die Erfolge dieser Studie hervorgehoben wurden, werden bestimmte Fallstricke erörtert. Die Beobachtungen wurden anhand von großen Mengen kategorischer Zeitreihenanalysen entdeckt. Um die Verarbeitung dieser Datenmengen zu vereinfachen, wurde ein Spezialwerkzeug entwickelt, welches in dieser Arbeit vorgestellt wird.

Schließlich wird ein Ausblick für dieses Projekt gegeben und dessen nächste Schritte präsentiert. Dank dem dynamischen Umfeld am CERN können durch bevorstehende Hardwareupgrades weitere Verbesserungen der Kostenfunktion in Aussicht gestellt werden.





## Acknowledgments

First and foremost, I would like to thank my supervisor Alexander Huschauer for his genuine efforts and tireless strive for excellence. I am truly grateful to have you as my supervisor. Thank you for your patience in the numerous attempts of teaching me about accelerator physics, for your trust in handling the machines, for your support, your constructive criticism and overall in your investment in my personal development.

CERN has been an extraordinary experience in my life which will forever stay with me. It has been an honour to meet and get to know so many remarkable people during this time. Thank you to the entire PS and PSB operations crew to make me feel welcome in the team and for the continuous support during my MD slots. Un grand merci à Marcel Coly, Marc Delrieux, Denis Cotte et Jean-Michel Nonglaton, qui m'ont aidé avec tellement de questions et de problèmes lié à SFTPRO. Thank you Sandy Easton, for sharing your knowledge on algorithms with me and for keeping the moral high with Joe McCarthy on long evenings in the control centre. Thank you Ron for showing me around in CERN's media team.

Thank you to Verena Kain, Nico Madysa and Michael Schenk for the numerous fruitful discussions on algorithms and optimisation techniques. Ein besonderer Dank geht heraus an Flavia Gehrig, für das gemeinsame Abenteuer ein Jahr am CERN zu verbringen und den wertvollen Austausch. Vielen herzlichen Dank an Hannes Pahl. Die unzähligen Gespräche beim Kaffee trinken und beim Mittagessen waren stets bereichernd. Egal ob privater, beruflicher oder schlicht persönlicher Natur.

Thank you in particular to my former flatmates, Rocco Ardino and Fabian Batsch. I could not have imagined any better welcome in the Geneva area. Thank you for the numerous fun & delicious evenings we spent cooking together and having a good time. Thank you for the trips we have done and for showing me the best spots in the area. Grazie mille Rocco. Vielen tausend Dank Fabian!

Finally, words cannot express how grateful I am to have these people in my life. Merci maman pour ton amour et ton support inconditionnel. Vielen Dank Susanne für deine Ratschläge, Ermutigungen und Unterstützung.

Vielen Dank Papa für all das, was du in mich hineingelegt hast. Ich vermisse dich.

Danke Matias, Danke Christoph, für die Unterstützung in dieser Zeit.

Vielen Dank Jonas, dass ich mich stets auf dich verlassen kann. Vielen Dank Chris, für die vielen Jahre als Freund und Ratgeber. Vielen Dank Martin, dass meinen Weg die letzten Jahre begleitet hast. Vielen Dank an die vielen Menschen in Karlsruhe, die mich die letzten Jahre begleitet haben!

Vielen lieben Dank Lina für deine liebevolle Art, weisen Worte und uneingeschränkte Unterstützung. Ich hätte mir niemals erträumen können, wie wertvoll es ist mit dir das Leben zu bestreiten und zu teilen.

**Post tenebras spero lucem.**



# Contents

<b>1</b>	<b>Introduction</b>	<b>13</b>
1.1	Beams and the Proton Synchrotron . . . . .	14
1.2	Motivation and goals . . . . .	15
1.3	Structure of the thesis . . . . .	16
<b>2</b>	<b>Environment</b>	<b>17</b>
2.1	Accelerator physics . . . . .	18
2.1.1	Fundamentals of an accelerator . . . . .	18
2.1.2	Magnets . . . . .	20
2.1.3	RF cavities . . . . .	21
2.1.4	Betatron Tune . . . . .	22
2.2	Accelerator operations . . . . .	23
2.2.1	Cycles and supercycles . . . . .	24
2.2.2	Trajectory along the accelerator complex . . . . .	26
2.3	The SFTPRO beam . . . . .	27
2.4	Technical frameworks & interfaces . . . . .	30
2.4.1	Optimisation interface and framework: COI and GeOFF . . . . .	30
2.4.2	Accelerator interfaces: CMW, JAPC & LSA . . . . .	31
2.4.3	Logging framework: NXCALS . . . . .	32
2.5	Algorithms . . . . .	33
2.5.1	COBYLA & BOBYQA . . . . .	33
2.5.2	Extremum Seeking . . . . .	35
<b>3</b>	<b>Preparation</b>	<b>37</b>
3.1	Initial conditions of this thesis and previous results . . . . .	38
3.2	Parameter grid search . . . . .	40
3.3	Problems with the existing cost function . . . . .	41
3.4	Implementing safeguards . . . . .	43

<b>4</b>	<b>Cost function design and algorithm tuning</b>	<b>44</b>
4.1	Milestone 1: core of the cost function . . . . .	45
4.2	Milestone 2: cost function weight for the TFB gain . . . . .	48
4.3	Milestone 3: cost function weight for the spill waveform . . . . .	51
4.4	Hyperparameter tuning . . . . .	53
4.5	Final demonstration . . . . .	54
<b>5</b>	<b>Conclusion</b>	<b>55</b>
5.1	External perturbations . . . . .	56
5.2	Supercycle dependency . . . . .	58
5.3	SST – Supercycle State Tracker . . . . .	59
5.4	Hypothesis concerning the source of perturbations . . . . .	61
5.5	Retrospective & final comparison . . . . .	62
<b>6</b>	<b>Outlook</b>	<b>64</b>
6.1	Future of SFTPRO: barrier bucket . . . . .	65
6.2	Improve the observables . . . . .	66
6.3	Future implementation . . . . .	69
<b>A</b>	<b>Appendix</b>	<b>70</b>
A.1	Correlation with MRP . . . . .	71
A.2	PS magnet layout . . . . .	72
A.3	GeOFF user interface . . . . .	73
A.4	SST examples . . . . .	74
<b>B</b>	<b>Bibliography</b>	<b>77</b>
<b>C</b>	<b>List of figures</b>	<b>82</b>
<b>D</b>	<b>Acronyms</b>	<b>84</b>

# 1



## INTRODUCTION

The *European Organization for Nuclear Research (CERN)* [1] began its mission of scientific discovery in 1954, with fundamental physics as its core business. Ever since, significant breakthroughs in particle physics and technology in general have been accomplished [2]. This work will combine domain knowledge in accelerator physics with the implementation of existing control and optimisation algorithms.

This work has been conducted in the course of the technical student programme of *CERN*.

### 1.1 Beams and the Proton Synchrotron

The work presented in this thesis took place in the *Proton Synchrotron (PS)* [4]. The *PS* is the oldest functioning accelerator in the accelerator complex at *CERN*, it has been accelerating particle beams since September 1959 [5]. A beam is the entity that consists of all particles circulating within an accelerator ring.

Accelerator research aims to produce beams that addresses the needs of fundamental scientific research in particle physics. Further applications include nuclear physics and biomedical sciences [6].

Evolving over the years, the *PS* still has an important role in the accelerator chain at *CERN*. In 2022 the *PS* was able to deliver a grand total of  $6 \times 10^{19}$  protons to the *Large Hadron Collider (LHC)* [4], the *Super Proton Synchrotron (SPS)* [4] as well as various fixed-target experiments [7].

The photograph in Fig. 1.1 shows the tunnel of the *PS* and its main components. The large blocks seen are the combined function main magnets, which are used to manipulate the beam along its trajectory in the ring. This image is shown to get an idea of the scale of this 628 m long machine and the numerous hardware components, which are required for operation [8].



Figure 1.1: The *Proton Synchrotron*. The photography is taken from [3].

## 1.2 Motivation and goals

Caused by phenomena such as temperature fluctuations or other effects, there are parameters that are subject to continuous drift in an accelerator. Currently, these phenomena are counteracted by operators working on shift throughout the physics production, this means that they need to identify the problem, understand it and act accordingly. The goal of this work has been to keep a certain parameter within well-defined limits.

Figure 1.2 shows the plot of such a drift. This example is taken from the problem that has been addressed in this presented study. The optimum of the value, which was the primary figure of merit focused in this work, is specified at  $n_{\text{MTE}}^{\text{optimum}} = 0.2000$ . As the trend of the fluctuating evolution of the value shows — substantiated by its rolling mean — the value is drifting away from its optimum. The dotted line in orange marks the range of acceptance, the range within the process is considered to be qualitatively sufficient.

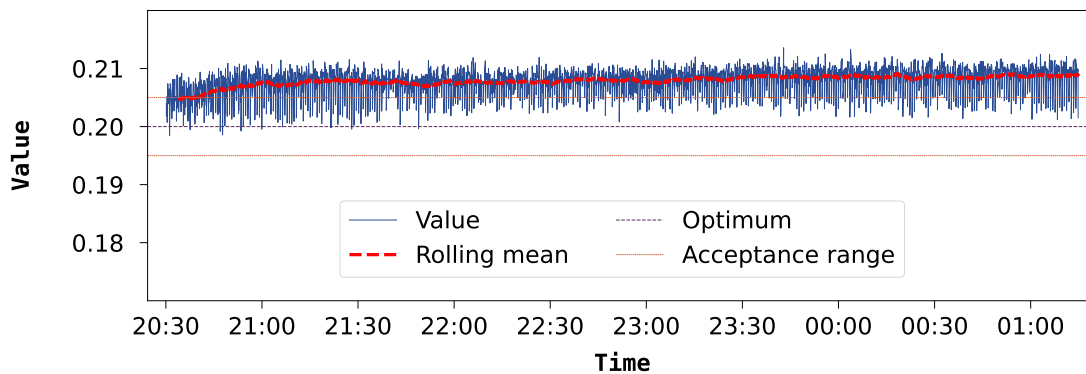


Figure 1.2: Exemplary drift to demonstrate the problem.  
The time series shown was recorded on 02 November 2022.

Figure 1.3 shows how the records taken from the physics production over the course of 2022. This data is again taken from the same subject that has been addressed in these studies. This representation enables to understand the distribution independently of fluctuations and nicely demonstrates where the centre of the Gaussian distribution is located. In fact, the median value of the dataset, represented by the red dotted line, is 0.1979.

The ultimate goal of this work will consist of getting this median value as close as possible to the optimal value of 0.2000.

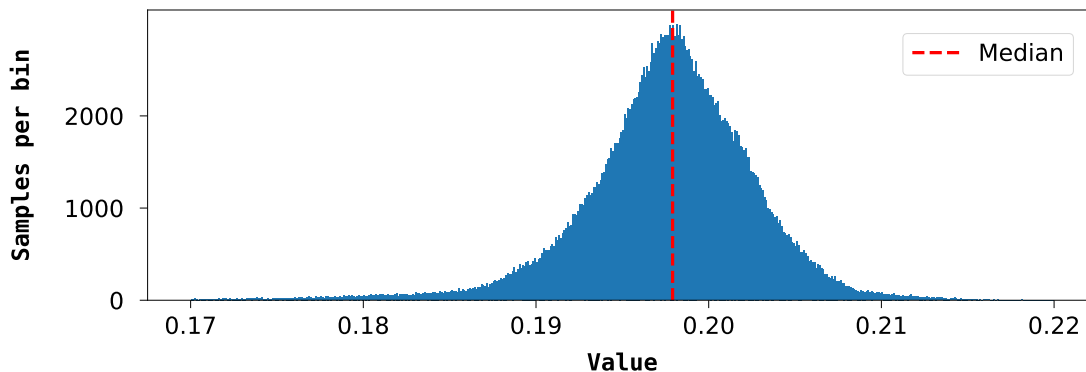


Figure 1.3: Distribution of beams used for physics production in 2022.

### 1.3 Structure of the thesis

Domain knowledge is key to explore and explain the data that will be considered during this work. Consequently, a major share of this work consists of building a knowledge basis on the subject. The first step will be a brief introduction into the world of accelerator physics and how the operation around accelerators is organised at *CERN*. Subsequently, these fundamentals pave the way to understand the beam that will be epicentre of this work.

Following this, a glance will be taken at the computational environment at *CERN* that will be used. This will overview the tools that have to be handled and will be accompanied by the algorithms that will be discovered and understood along this journey.

Having cleared the obstacles, it will be time to state the initial conditions imposed by this work at hand, before being able to eventually start the development process. The development will be carried out in an iterative manner in a bottom–up approach to ensure the efficacy of the individual steps during the progress.

Finally, to wrap up the work, the final observations made during the development are laid out. These will subsequently allow to give an outlook and final evaluation of this work.



# 2



## ENVIRONMENT

In this section, the various components required for the comprehension of this work are presented. Given the broad scope of the task, the information will be presented briefly as the components make up entire areas of research on their own. The challenges encountered during the development originate primarily from the broad spectrum of aspects that need to be taken into consideration for this work to become successful.

## 2.1 Accelerator physics

A rough understanding of accelerator physics is prerequisite for this work. This will provide the correct basics to interpret the data analysed in the framework of this project.

Most information summarised in this section, unless explicitly stated otherwise, is taken from [9]. [9] in itself is a summary from an introductory course to accelerator physics. [9] is often given to operators and newcomers at *CERN*, who typically do not have any experience in accelerator physics prior to starting their work [10].

### 2.1.1 Fundamentals of an accelerator

**Notation** To start with, a definition of the notation used to describe the movement of particles within an accelerator is given. The following Fig. 2.1 depicts this. The longitudinal coordinate  $s$  describes of the location of a particle within the accelerator ring. The displacement along this direction is commonly described by the azimuth  $\theta$  ranging from 0 to  $2\pi$  [10].

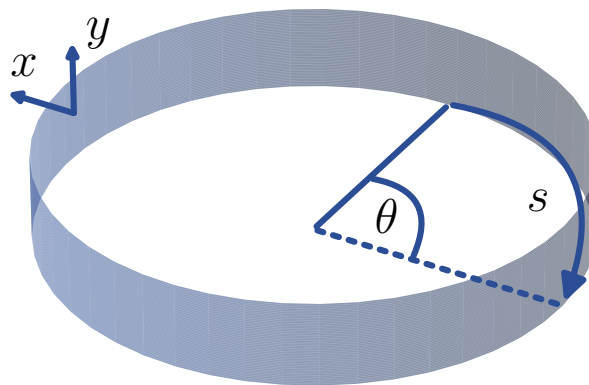


Figure 2.1: Coordinate system within an accelerator ring.

The transverse motions, which consists of both the horizontal and vertical motions, occur perpendicular to the longitudinal motion. The horizontal movement is described by  $x$  and the vertical movement by  $y$ . In addition to its physical position, the transverse motions are supplemented with its angle in respect to  $s$ ,  $x'$  and  $y'$  respectively.

The coordinates  $x$ ,  $y$  and  $s$  can be thought of as the cartesian coordinates of a particle at any location within the accelerator [10].

**Beam** The particles within a beam need to be charged in order to be manipulated. For the scope of this work, only protons will be considered.

The beam can be either bunched or debunched. Bunched means that the particles are separated in time into packages of particles [11]. A debunched beam refers to particles that are distributed continuously along the accelerator. The intensity of a beam, i.e., its number of particles, is commonly measured with beam current transformers (BCTs) [12], and expressed in terms of  $10^{10}$  charges in the *PS*.

To explain the (transverse) emittance, consider Fig. 2.2. The emittance is the surface area of the resulting ellipse, which contains all or a defined percentage of the particles [13]. The increase in emittance is coupled with an increase in size of the beam [14], which is undesirable.

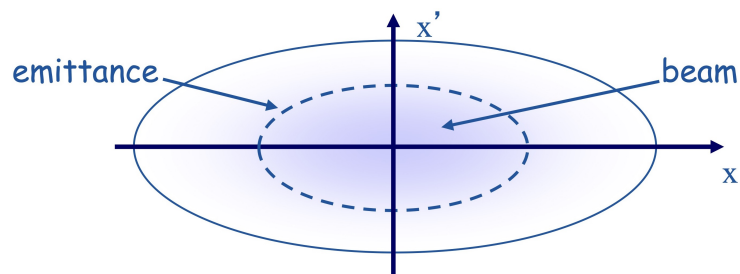


Figure 2.2: Transverse emittance in phase space<sup>1</sup>. The graphics is taken from [13].

**Structural elements** While the *PS* also consists of multiple more sensor and actuator devices, the following description will be limited to the structural elements to manipulate the particles within an accelerator. The vacuum chamber is a toroidal tube, which forms the ring and is the transport medium of the particles. The vacuum chamber is then surrounded by different types of magnets, used to control the trajectory in both the longitudinal and transverse planes. These will be presented in Section 2.1.2. To accelerate the particles, so-called radiofrequency (RF) cavities are used. RF cavities will also have their dedicated section, Section 2.1.3.

<sup>1</sup>More on phase spaces in [15].

### 2.1.2 Magnets

The *PS* ring consists of 100 combined–function magnet units, which create dipolar and quadrupolar magnetic fields [10]. The magnets are used to control and steer the beam while it traverses the accelerator. A sketch of the *PS* layout including the arrangement of the combined–function magnets can be found in the appendix.

In modern accelerators, separate function magnets, i.e., individual dipole and quadrupole magnets are used. Thanks to a smart design and wise engineering choices when the *PS* was built in 1950s, the configuration remains operational until this day [5].

**Dipoles** Electromagnet with two poles. It is responsible for the bending around the accelerator ring. The dipole field is homogenous along the full magnet and bends the ring for  $3.6^\circ$  [10]. The resulting magnetic field has a linear impact on the particles.

**Quadrupoles** Electromagnet with four poles. Also induces linear effects. It is used to focus and defocus the beam, which is achieved in alternating the polarity of the magnets. The quadrupole magnets ensure that the transverse motion takes place inside the vacuum chamber [10].

**Sextupoles** Again adding two more poles to a magnet result in a sextupole. This time the implications are more intricate. The effects that are induced by the involved fields are now nonlinear which greatly increases the complexity of calculations involved when designing an accelerator. Generally, they are used to control the so–called “chromaticity” (see [16]), which will not be elaborated any further in this work [10].

**Octupoles** Electromagnet with eight poles, which also induces nonlinear effects.

**Hysteresis** Hysteresis is a phenomenon in ferromagnetic materials. For a magnet to be magnetised, a magnetic field must be applied to it. To reset the magnetic field, a magnetic field in the opposite direction has to be applied. However, due to hysteresis the magnetic field will not be reset to zero and a small remanent magnetic field will remain [10].

Hysteresis is a deterministic process that depends on the magnetic field<sup>2</sup> and is invariant regarding time scaling [17].

---

<sup>2</sup>Also called “*B*–field”.

### 2.1.3 RF cavities

Now that it is clear how to move in the transverse plane, the key device used to accelerate the particles is presented: the RF cavity.

In the *PS*, the RF cavities will accelerate the beam to its terminal velocity. As the speed increases, adapting the frequency of the RF cavity to the increased speed is crucial.

Once the beam passes through the RF cavity, it will be exposed to an electrical field in a narrow gap in the vacuum chamber, as pictured in Fig. 2.3. The field is generated by two electrodes, which are separated by the narrow gap. Powered by an alternating current (AC) circuit, the field then switches polarity at high frequencies [10].

RF cavities operating in different frequency range have different tasks. In the *PS*, there are multiple types of cavities installed. For this work, the “10 MHz cavities” will play an important role. The 10 MHz cavities operate at frequencies between 2.8 and 10 MHz [18].

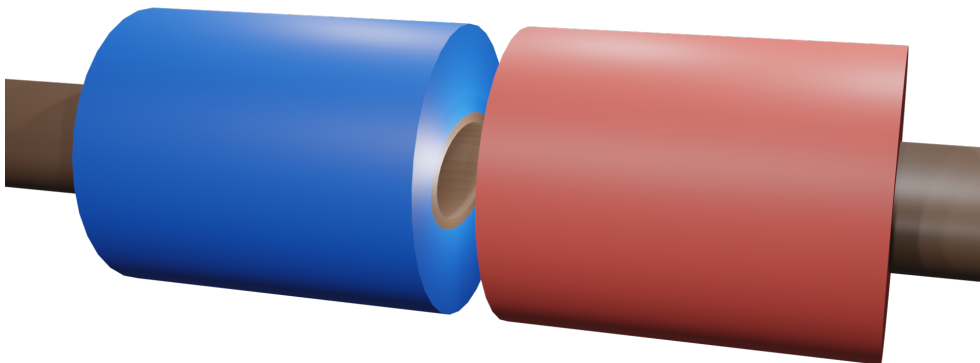


Figure 2.3: Demonstrating the idea of an RF cavity.

The brown tube represents the vacuum chamber.

In red and blue are the electrodes of the cavity, which alternate during operation.

The particles are accelerated within the air cap, visible between the electrodes.

### 2.1.4 Betatron Tune

The tune, commonly referred to as “ $Q_{x|y}$ ”, is the number of transverse oscillations of a particle per turn in the machine. The betatron oscillation describes the frequency at which a single particle oscillates within the horizontal ( $Q_x$ ) and vertical ( $Q_y$ ) plane. The tune is defined by the arrangement and strength of the focusing and defocusing of the quadrupole magnets. As the tune is directly linked to the interaction of the particles with the  $B$ -field, it can be perturbed by hysteresis effects.

Imagine a single particle as a ball rolling in a half-round gutter, like in Fig. 2.4. Using this picture, one oscillation of the ball is the counterpart of one betatron oscillation. The quadrupole magnets act as the gutter, which defines the trajectory of the ball. The number of oscillations per gutter, i.e., per turn in the accelerator, is the tune. These characteristics correspond to betatron oscillations of particles within a circular particle accelerator.

To operate the tune in  $PS$ , a control setting, which controls the strength of auxiliary small quadrupole magnets, slightly shifts the tune at discrete, specified moments is used. This setting will be used extensively throughout this work and is one of the actuators used in the experiments.

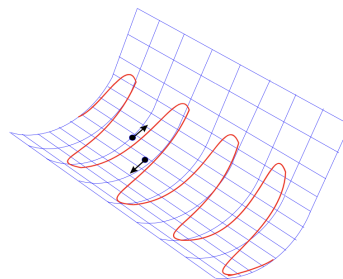


Figure 2.4: Motion of a ball in a half-round gutter. The graphics is taken from [9].

**BBQ** Knowing what a betatron oscillation represents, the next step is to understand how to measure it. For this feature, a method called base band tune (BBQ) is utilised, which is implemented in a homonymous application. The BBQ utilises a diode detector to determine the transversal position of the beam along the ring [19]. The acquired positional data is then fed into a *Fast Fourier Transform (FFT)*, which is then outputs the signal into a frequency.

The BBQ application allows to narrow down the data fed into the *FFT* to specify at which point as well as how many turns during the cycle the frequency shall be determined.

## 2.2 Accelerator operations

Generally, this section will be dedicated to the constraints and procedures related to the operation of the *PS* accelerator. The first part is intended to give a better idea of how the operation in general takes place and what conditions are imposed in particular regarding schedule. Fig. 2.5 shows a typical day at the core of machine operation at *CERN*, the *CERN Control Centre (CCC)* [4]. It is here that the majority of this work was carried out and supported by the entire group responsible for the *PS*.

At the *CCC*, all major accelerators at *CERN* are controlled. This concerns the *LHC*, *SPS*, *PS*, *Proton Synchrotron Booster (PSB)* [4] and *Linac4* [20], which all have their respective teams dedicated to operation. Each team of operators works on shifts to guarantee the readiness of the accelerators day and night, for every day between their restart and shutdown. The restart and shutdown of the accelerators are delimited by either type of event:

- The year-end technical stop (YETS), which occurs yearly and in 2022, started on 28 November. The YETS allows for minor upgrades to the accelerator hardware.
- The long shutdown (LS) is used for larger projects in the accelerators. Most recently, during the so-called LS2, the *LHC injectors upgrade (LIU)* project was conducted. LS2 prepared the *PS* for operation until the 2040s.



Figure 2.5: A typical day in the *CCC*. The photography is taken from [21].

### 2.2.1 Cycles and supercycles

A cycle is a collection of settings for a given beam. The beams in the *PS* are either sent to an experiment directly, to the *SPS* or dumped. Cycles are typically identified by their timestamp at the beginning of the cycle, the “cyclestamp”. The cycles themselves are referred to by their “*LSA Cycle*” name, which commonly have a superordinate beam type, e.g., *LHC*–type beam. A beam is either used for physics production or for development purposes, the latter are called “machine development (MD) beams”. The planning for MD beams is managed in three slots throughout one day. The beam that will be used in this work will hereby be referred to as “the MD beam”.

A beam conveys a certain particle type. To date the events taking place within a cycle, the cycle time ( $t_c$ ) is used.  $t_c$  describes the millisecond since the start of the cycle. A cycle is made up of one to three basic periods (BPs); 1 BP is 1200 ms long. Cycles are configured within a sequence called the supercycle (SC). Within the SC, the cycles can either be configured as a primary or spare cycle. This distinction allows the alternate between the primary and spare cycle without modifying the current SC configuration. A SC is repeated indefinitely until the operators update it according to current requirements of the physics users or other circumstances. To index the individual cycles within a SC, both cycle and BP index are stated. This distinction is important as a 3 BP long primary cycle, incrementing the cycle index by 1, could be replaced by 3 spare cycles with 1 BP, which increments the cycle index by 3. Whenever a SC is updated, the SC counter is reset to 1.

The cycles themselves are commonly visualised by the  $B$ –field of the magnets, i.e., their magnetic field. This visual representation, pictured in Fig. 2.6, is able to quickly convey the state of the SC to trained

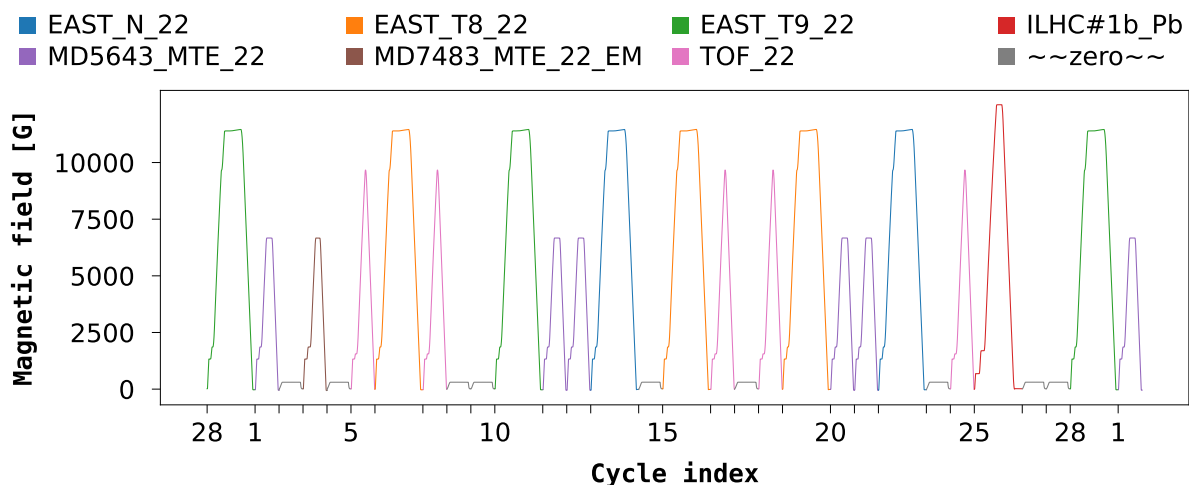


Figure 2.6: Visualisation of a supercycle.



observers. Additionally, it allows to quickly identify potential hysteresis problems induced by preceding cycles as the hysteresis is linked to the  $B$ -field [10].

Table 2.1 has been curated to showcase how diverse a single SC can become. The amount of categorical information, which is continuously generated and published by the “timing server”, has frequently caused obstacles during the course of this work. To put this into perspective: this table merely covers 36 seconds of operation in the *PS*.

Cyclestamp	SC	Cycle	BP	LSA Cycle	Destination	ms	Particle
03:44:21	86	28	35	EAST_T9_22	EAST_T9 NTOF	2400	PROTON
03:44:23	87	1	1	MD5643_MTE_22	TT2_D3	1200	PROTON
03:44:24	87	2	2	~~zero~~	PS_DUMP	1200	NOBEAM
03:44:25	87	3	3	MD7483_MTE_22_EM	TT2_D3	1200	PROTON
03:44:27	87	4	4	~~zero~~	PS_DUMP	1200	NOBEAM
03:44:28	87	5	5	TOF_22	NTOF	1200	PROTON
03:44:29	87	6	6	EAST_T8_22	EAST_T8 NTOF	2400	PROTON
03:44:31	87	7	8	TOF_22	NTOF	1200	PROTON
03:44:33	87	8	9	~~zero~~	PS_DUMP	1200	NOBEAM
03:44:34	87	9	10	~~zero~~	PS_DUMP	1200	NOBEAM
03:44:35	87	10	11	EAST_T9_22	EAST_T9 NTOF	2400	PROTON
03:44:37	87	11	13	MD5643_MTE_22	SPS	1200	PROTON
03:44:39	87	12	14	MD5643_MTE_22	SPS	1200	PROTON
03:44:40	87	13	15	EAST_N_22	EAST_N NTOF	2400	PROTON
03:44:42	87	14	17	~~zero~~	PS_DUMP	1200	NOBEAM
03:44:43	87	15	18	EAST_T8_22	EAST_T8 NTOF	2400	PROTON
03:44:46	87	16	20	TOF_22	NTOF	1200	PROTON
03:44:47	87	17	21	~~zero~~	PS_DUMP	1200	NOBEAM
03:44:48	87	18	22	TOF_22	NTOF	1200	PROTON
03:44:49	87	19	23	EAST_T8_22	EAST_T8 NTOF	2400	PROTON
03:44:52	87	20	25	MD5643_MTE_22	SPS	1200	PROTON
03:44:53	87	21	26	MD5643_MTE_22	SPS	1200	PROTON
03:44:54	87	22	27	EAST_N_22	EAST_N NTOF	2400	PROTON
03:44:57	87	23	29	~~zero~~	PS_DUMP	1200	NOBEAM
03:44:58	87	24	30	TOF_22	NTOF	1200	PROTON
03:44:59	87	25	31	ILHC#1b_Pb	TT2_D3	2400	PB54
03:45:01	87	26	33	~~zero~~	PS_DUMP	1200	NOBEAM
03:45:03	87	27	34	~~zero~~	PS_DUMP	1200	NOBEAM
03:45:04	87	28	35	EAST_T9_22	EAST_T9 NTOF	2400	PROTON
03:45:06	88	1	1	MD5643_MTE_22	SPS	1200	PROTON

Table 2.1: Example of a single supercycle (plus its preceding and succeeding cycle).  
Detailed representation of the SC pictured in Fig. 2.6.  
Data recorded on 31 October 2022.

### 2.2.2 Trajectory along the accelerator complex

The purpose of this section is twofold. Figure 2.7 provides an overview of all possible trajectories and destinations of beams at *CERN*. Additionally, it shows where the source of the potential perturbations that impact the MD beam prior to reaching the *PS* is located.

The MD beams are created in the *Linac4* and are subsequently injected into the *PSB*. After acceleration in the *PSB*<sup>3</sup>, the beams are transferred to the *PS*. Once the beam is finished its stage in the *PS*, it will be ejected through the transfer line “*TT2*” [23], where it will reach an intersection with two possibilities. For the purposes of the development, the beams are dumped in the next step. The operational equivalents of the MD beams are sent to the *SPS* in their next step. In the *SPS*, they will be accelerated further before being used in *CERN*’s *North Area* (*NA*) [24] for fixed-target physics.

The complexity of the infrastructure enables a vast possibility for perturbations ahead of time. Therefore, the injected beam quality into the *PS* was actively monitored while performing beam studies. This ensured that issues were detected ahead of time to avoid feeding corrupted data into the algorithms.

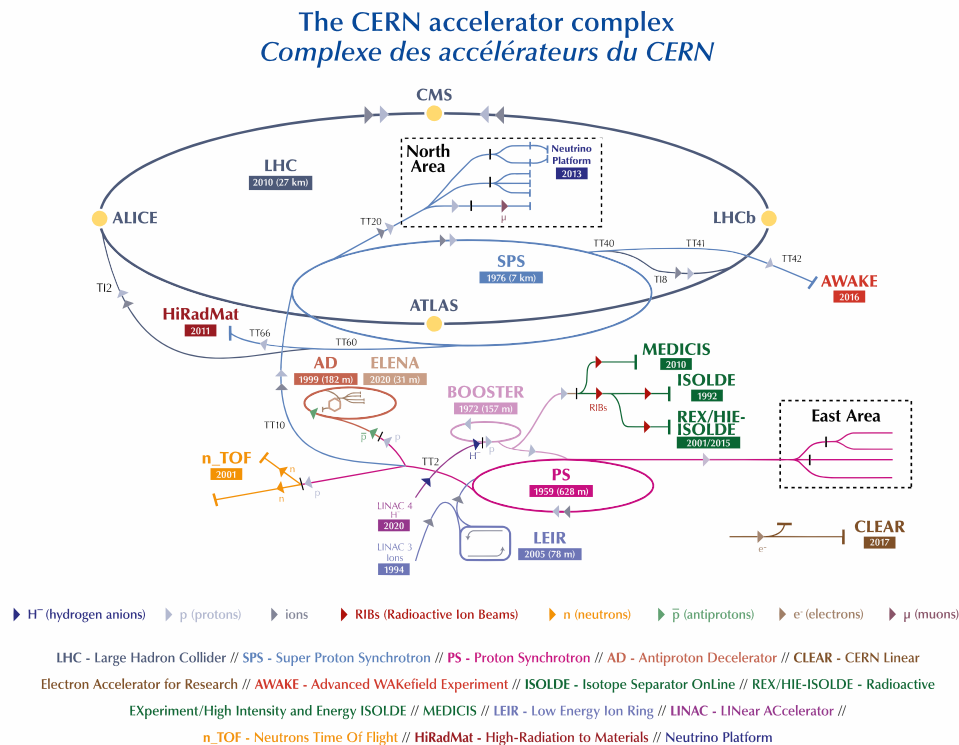


Figure 2.7: Overview of the *CERN* accelerator complex. The graphics is taken from [22].

<sup>3</sup>Referred to as “BOOSTER” in Fig 2.7.

### 2.3 The SFTPRO beam

After introducing the different building blocks representing the basics of accelerator physics as well as the operational basics of accelerators at *CERN*, it is now time to discuss the details about the type of beam used for the MD beam: the SPS fixed target protons (SFTPRO) beam. This beam uses a novel type of beam production, the multi–turn extraction (MTE), that has been put in operation in 2015 [25].

MTE was developed to reduce beam loss during the extraction process. This is achieved by splitting the beam in horizontal phase space into 5 beamlets. Figure 2.8 shows the horizontal phase space before and after the splitting process. The beamlet at the centre of the phase space in Fig. 2.8b is called core. The four remaining beamlets, located on the outskirts, are called islands. This splitting is achieved by applying nonlinear magnetic fields induced by sextupoles and octupoles. The distance from the origin of the islands is proportional to the horizontal tune [10].

Once the beam is ejected from the *PS*, its intensity is measured in a single point in *TT2* during its transfer. The measurement consists of  $\sim 600$  consecutive samples. As the samples are naturally separated by time, each sample therefore measures a fraction of the beam along its total length. The plot of the vector of samples makes up the “extraction spill”. The spill is subsequently used to assess the quality of the extraction in two aspects:

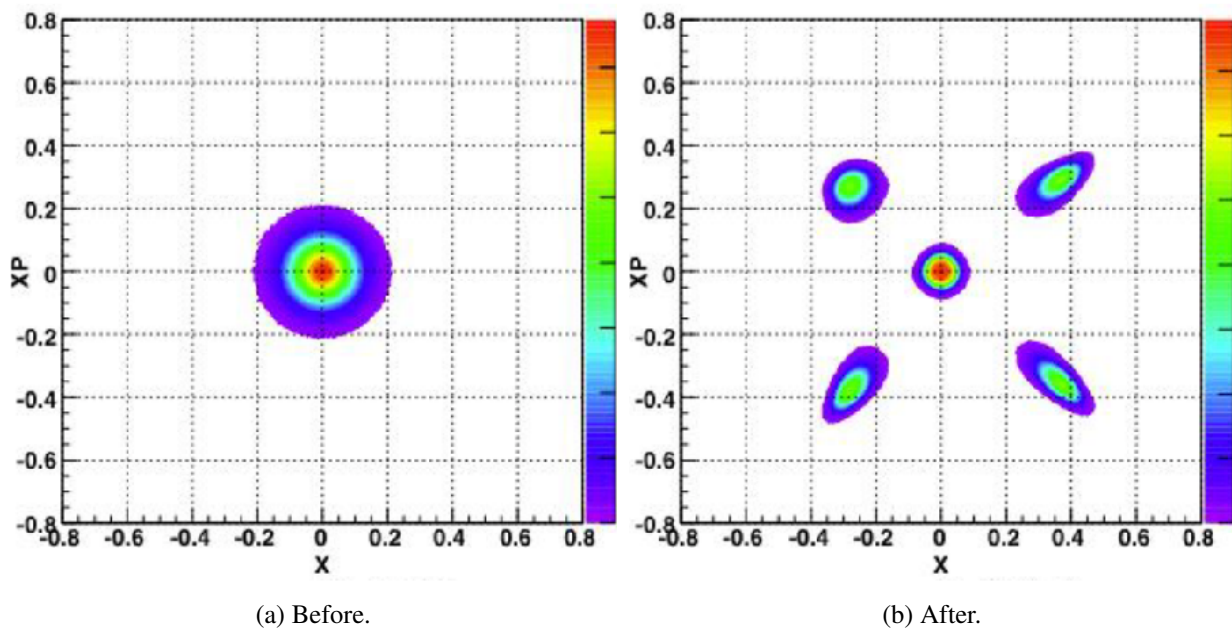


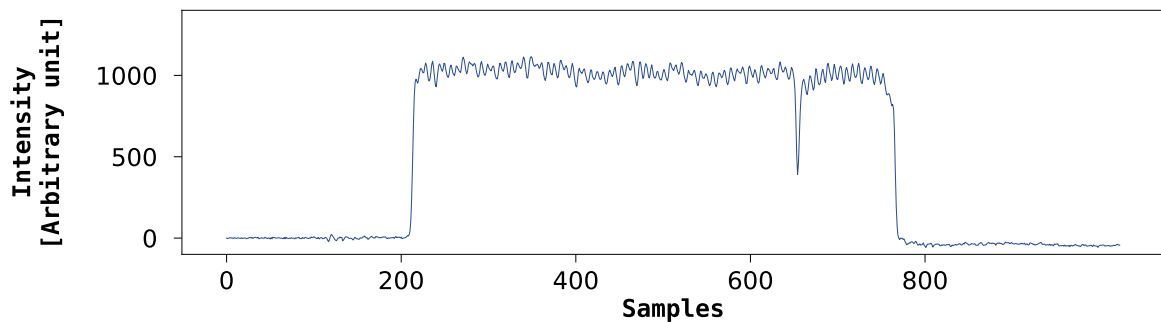
Figure 2.8: Simulation of the beam before and after the splitting process. The graphics is taken from [26].

### 2.3 The SFTPRO beam

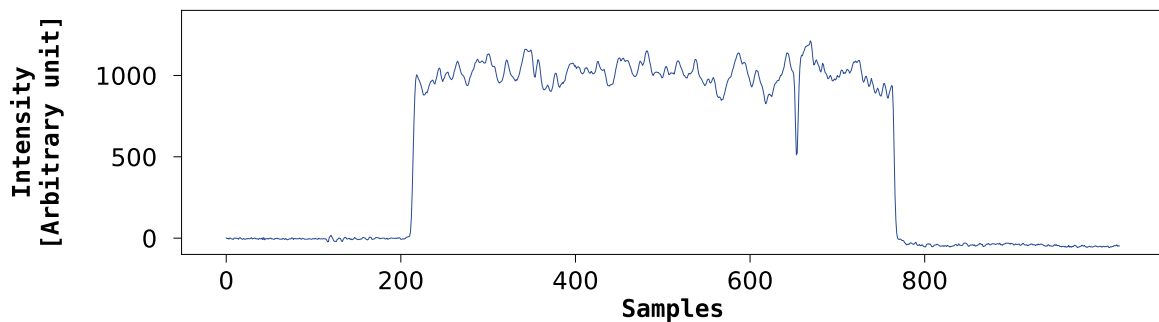
---

- The MTE efficiency<sup>4</sup> expresses how well the five beamlets have been split. This figure of merit ideally equals 0.2000, as this expresses that every beamlet makes up 20.00% of the total beam intensity. It is defined as  $MTE\ efficiency = n_{MTE} = \frac{\langle I_{Islands} \rangle}{I_{Total}}$  where  $\langle I_{Islands} \rangle$  is the average intensity in each island and  $I_{Total}$  the total beam intensity [27].
- The waveform of the spill should be as uniform as possible, i.e., squared, in order to maintain a uniform flow of protons for the fixed-target experiment.

Figure 2.9 shows an example of a good and a bad spill.



(a) Example of a good spill.



(b) Example of a bad spill.

Figure 2.9: Example of a good and a bad spill.

---

<sup>4</sup>Sometimes referred to as “splitting ratio” or simply “ratio”.

Notable timestamps within the SFTPRO cycle are injection at  $t_c \approx 170$ , ejection at  $t_c = 835$  and the splitting, which takes place between  $t_c \cap [720; 830]$ . Figure 2.10 shows the timeline of the splitting.

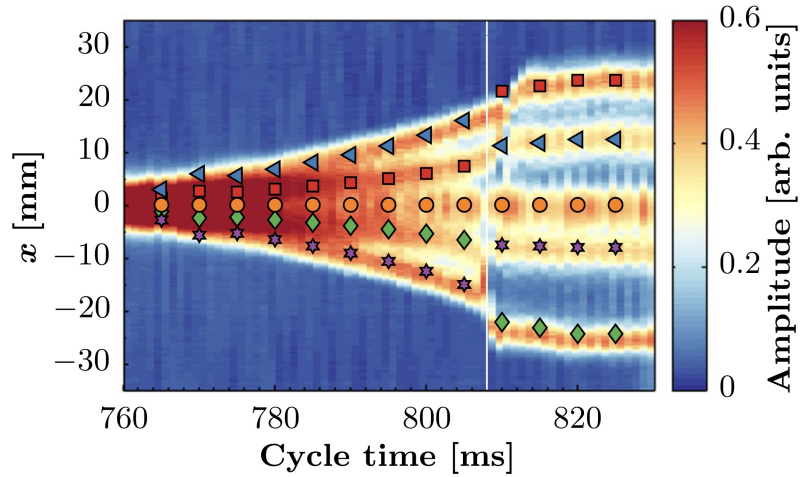


Figure 2.10: Timeline of the MTE splitting. The graphics is taken from [27].

**TFB** The transverse feedback (TFB) system is used to correct unstable beam motion in the transverse plane [10]. There are several caveats attached to this system which played a crucial role towards the performance of the MD beam.

Two properties of the TFB are important for these studies. The system has to operate at a specific frequency, controlled by the “TFB harmonic”. Additionally, the strength of the system, the “TFB gain”, has to be rationed wisely. The TFB gain will typically increase the ratio, the principal figure of merit that will be considered in this work. Simultaneously, the transverse emittance of the beam is increased.

Alongside the tune, the TFB gain and the TFB harmonic will be the primary actuators considered throughout this work.

### 2.4 Technical frameworks & interfaces

The following part is dedicated to explain the various frameworks used for this project. This is done to put matters into perspective in order to comprehend the benefits and potential caveats encountered over the course of the work. An overview of how the frameworks are intertwined is given at the end of the section in Fig. 2.11.

#### 2.4.1 Optimisation interface and framework: COI and GeOFF

**COI** The *Common Optimization Interface (COI)* is a framework developed at *CERN*. Its aim is to create an interface for various numerical optimisation problems, machine- and reinforcement learning tasks [28]. The package is based on the *Gym* environment [29], which allows any developer familiar with this popular package to be able to orientate themselves quickly and create their own custom environment.

In fact, the code that was developed to run the online optimisation will inherit from the base classes [30] provided by the *COI* package.

**GeOFF** The *Generic Optimization Frontend and Framework (GeOFF)* is a graphical user interface (GUI) for *COI* [31], which bundles frequently required actions in a user-friendly way. It couples the required middleware for communication with the remaining infrastructure of the accelerators with easily configurable scripts from *COI*. Additionally, the GUI features plotting windows to track the evolution of the actuators and the cost function of a given optimisation problem. The plots provide instantaneous feedback to developers that are monitoring an optimisation episode.

In order to facilitate the development of optimisers even further, numerous widgets from a *CERN* internal library to interface the accelerators are implemented [32]. These provide actions such as selecting the correct cycle. Additionally, *GeOFF* allows modifying variables from the *COI* script within the GUI, offers various implementations of algorithms which are selectable in a drop-down menu or provides a logging console to monitor the output of the *COI* script. The logs are stored for post-mortem analysis of the flow of actions to allow tracking experiments that span over several days.

*GeOFF* is the application that was used primarily when running the various experiments that made up this work. A screenshot of it is included in the appendix.

### 2.4.2 Accelerator interfaces: CMW, JAPC & LSA

**CMW** The *Controls Middleware (CMW)* is a middleware that was developed at *CERN* for the operation of the *LHC* [33], which is now used across the entire accelerator complex. It is placed between devices and clients. The devices are treated as servers and the *CMW* is based on the publish/subscribe paradigm.

Devices can be either physical or virtual and are used to control and monitor the state of the accelerators. The clients consist of both the controlling software in the *CCC* as well as application programming interfaces (APIs) to facilitate rapid prototyping for researchers [33].

**JAPC** The *Java API for Parameter Control (JAPC)* is one of the available APIs provided in order to communicate with the *CMW* [34]. It forms the foundation of one of the key tools of this project: the *PyJapc* package [35].

*PyJapc* is a *Python* [36] library which interacts with *JAPC* to provide native *Python* access to most commonly used operations such as a get & set on parameters or handling a subscription. Authorisation and authentication with the system is also provided [35].

**LSA** The *LHC Software Architecture (LSA)*<sup>5</sup> is the database architecture that is used to run the accelerators at *CERN* [37]. Abstracting the communication layers, its usage can be pictured as an online interface between the operators and the machines themselves. Typically, another level of controls application will be added in between the operators and *LSA* itself.

This persistence layer of low- and high-level settings forms the backbone of the operations of the machines. In addition to storing the current parameters, *LSA* provides a version history of tweaked settings, which makes a heuristic approach in controlling the accelerators possible [38].

The typical workflow for the experiments carried out in this project consisted of running an optimisation using *GeOFF*, followed by monitoring the updates in an *LSA* GUI and rolling back changes as required. Also featured in the versioning are both comments and tagging of parameter tuples to make navigation more efficient as well as less prone to human error. Therefore, the intentional design to make heuristic approaches possible will directly be applied in the studies presented in this work.

---

<sup>5</sup>Pronounced “Elsa”.

### 2.4.3 Logging framework: NXCALS

The *Next CERN Accelerator Logging Service (NXCALS)* is the service used for data logging within the *CERN* accelerator complex [39]. The data storage layer — the backbone of the system — is implemented with *Apache Hadoop* technology for distributed processing of large data sets. This allows to achieve a reliable and scalable infrastructure to meet the performance requirements handling such large amount of data [40]. The data to be stored at the end of 2018 was within the range of 2.5 TB / day [39].

In order to interface the *Apache Hadoop* cluster, *NXCALS* provided support for *Apache Spark*, which provided a robust framework to process the acquired data [41]. This allowed for detailed and long-term exploratory data analysis (EDA), which will be used later in this work.

The layer to *Apache Spark* is then finally interfaced in *Python* using *PySpark* [42]. This will be the layer that was utilised for EDAs that were carried out after conducting the experiments.

During the course of this work, several waveforms that are sampled up to 0.1 kHz are used, such as the voltage acquisition of the RF cavities. Simply considering the 10 MHz cavities, which are the main accelerating cavities in the *PS*, there are 11 of them installed.

To expand the picture about the vastness of data, the MD beam alone is considered first. The 46 087 times the cycle was executed over the course of the year summed up to a total of 55304.4 seconds. This is about 30 times less than the operational beam. Assuming 64-bit floating-point numbers, one device alone will have taken up 4.4 GB of data.

Using *Apache Spark DataFrames* made it technologically possible to treat the data as one entity without having to handle the overhead that comes from having to do manual partitioning.

Finally, Fig. 2.11 shows how the different components that were presented are linked together.

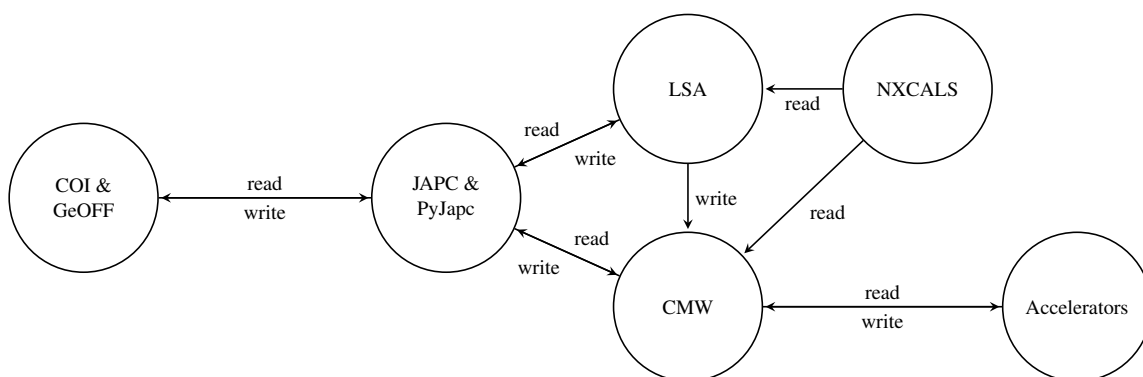


Figure 2.11: Flowchart of the technical frameworks and interfaces.



## 2.5 Algorithms

To conclude the section about the environment of the presented work, this part is dedicated to the various algorithms that were tested and used for this project. All of them are commonly used at *CERN* and implemented within the *COI* interface presented in Section 2.4.1.

### 2.5.1 COBYLA & BOBYQA

The two distinct algorithms share many characteristics and are therefore explained in the same section and immediately compared to one another. They were both developed by M. J. D. Powell. They are both derivative-free optimisation approaches that work by seeking the minimum value of an objective function. They are both iterative approaches.

Aside from their algorithmic characteristics, the choice of the appropriate algorithm is also related to its available implementation and their choice of hyperparameters [43].

**COBYLA** Developed in 1994, the *Constrained Optimization BY Linear Approximation (COBYLA)* algorithm works by finding the minimum value of a cost function using linear approximation [44]. A thorough example of the method of linear approximation is found in [45].

Essentially, the algorithm works by launching an exploration phase of the variables to establish the values of the cost function. Then the point with the minimum value is chosen. The subsequent minimum is then computed using linear approximation. This last step is repeated until no further improvements are made.

Additionally, *COBYLA* supports a constraint function which can be used to increase the reliability of the algorithm. The main drawback of this approach is that it can only work efficiently for functions up to 9 variables due to the nature of the linear approximation [44]. This however was not an issue in the problem of this work, knowing that a maximum of 3 actuators / variables was inspected.

**BOBYQA** Similar to *COBYLA*, the *Bound Optimization BY Quadratic Approximation (BOBYQA)* algorithm also seeks the minimum value of a cost function [46]. The algorithm also starts with an exploration phase of the variables in use [47].

The key difference is that the degree from the approximation is raised from a first degree (linear) approximation to a second degree (quadratic) approximation. Or simply put, the cost function is approached by a parabola instead of a line [48].

**Comparison** The *COBYLA* implementation is based on the popular *Python* package *SciPy* [49]. This package provides few additional features besides the minimal implementation of the algorithm as proposed by Powell.

*BOBYQA* on the other hand, is based on the package *Py-BOBYQA* [50]. The main benefit for this project was the plethora of implemented optional arguments that facilitated the development of this project [51].

**Final choice of optimiser** The *BOBYQA* implementation was eventually chosen for this work as a mean to try out optimisation methods. In particular, the feature to set the number of samples per step of the optimiser was used extensively. While it would not have been difficult to extend this functionality to *COBYLA*, no other benefits were apparent which substantiated the decision to pursue the use of *BOBYQA*.

Any of the optimisers themselves will not be applied towards the ultimate goal of this project. Instead, they will be leveraged to greatly reduce the development time required to validate the design of the cost function.

**Hyperparameters** The value range of the actuators is the key hyperparameter considered across all different algorithms.

Unique to *BOBYQA*, the parameter “`nsamples`”, which allows to set the number of samples per step, will be of use to counter the noisy nature of the MTE beam.

### 2.5.2 Extremum Seeking

*Extremum Seeking (ES)* is the key algorithm considered for the autonomous splitting control of the SFTPRO beam in the *PS*. It belongs to the category of closed-loop feedback controllers, as pictured in Fig. 2.12, which generally blend in with techniques from optimisation [52].

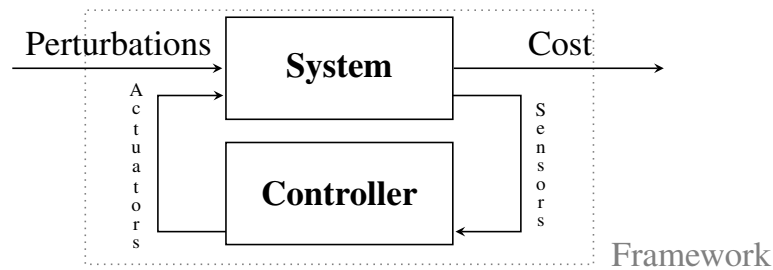


Figure 2.12: Standard framework for a closed-loop controller [53].

While the idea of *ES* as a control application dates back to the 1940s, it has resurged as a research topic since the 1990s as mean for real-time optimisation in industrial applications [54]. This version of the *ES* algorithm used in this work is one of many approaches to control unknown time-varying systems.

**Principle** The principle of the *ES* algorithm is to closely track the value of the optimal cost function [55]. This is achieved by assigning a dithering frequency [56] for each actuator to be set. The algorithm slowly adapts the amplitude of the oscillation of its actuators after each period towards the minimum of the cost function. While the shape of the frequency is expected to be sinusoidal by design, it has been demonstrated that the various classes of different dithering techniques result in identical average system dynamics [57]. The disjoint frequencies and the shape of the oscillation can be seen in Fig. 2.13b.

**Conditions** In order for the algorithm to function, following conditions must be met:

1. The iterations of the system must be reinitialised repeatedly with identical conditions<sup>6</sup>.

This means that the external conditions between the iterations of the system, i.e., between the steps while the algorithm is being executed, should not be altered.

Certain cycles are known to cause issues when executed before the SFTPRO cycle. During specific measurement periods, it was requested to restrict the SC configuration in order to not violate this

<sup>6</sup>This is not to be confused with the initial conditions of the system. The initial conditions refer to the state of the system before the algorithm is launched and can be different.

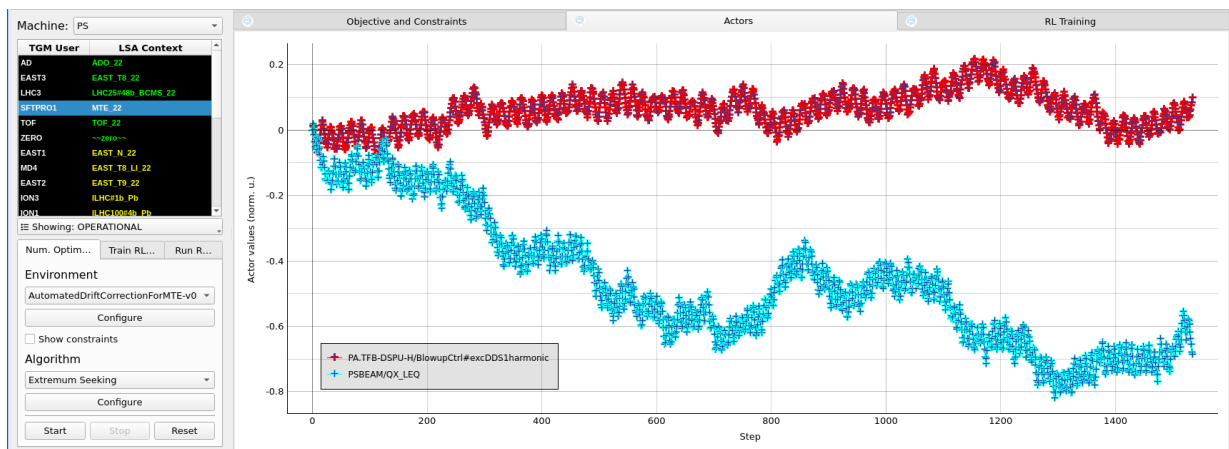
## 2.5 Algorithms

restriction deliberately. In the fast-paced environment at the *PS*, this request was not able to be respected continually. As anticipated, these real-life conditions caused problems for the *ES* algorithm and these scenarios will have to be closely inspected further.

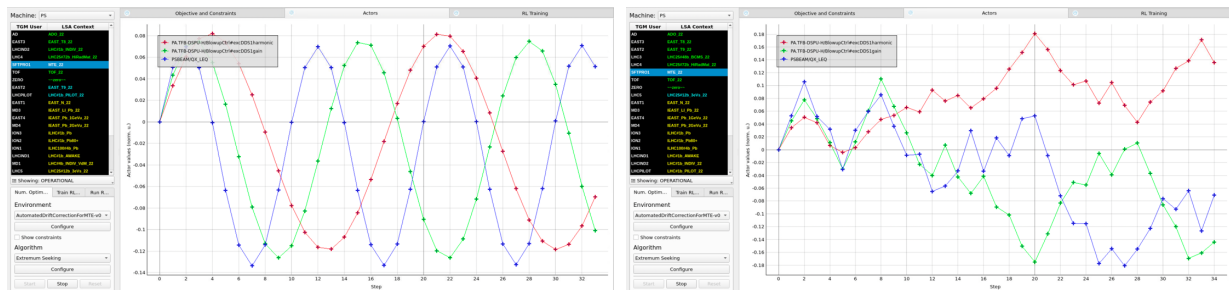
2. The cost function must be convex or linear.

**Hyperparameters** The hyperparameters for this application of *ES* are the following: gain and oscillation amplitude. The oscillation amplitude is self-explanatory: this reduces the absolute values that the actuator will be set to. This parameter is tuned to be balanced between a too low setting, which can make the effects on the system negligible; and a setting that is too high, which will tamper the system.

The gain on the other hand is a factor added to the input of the cost-function. Using the gain, it is possible to tune the numerical stability [58] of the controller. The implication of the gain is best demonstrated in the following Fig. 2.13. The gain was set to 0.02.



(a) Expected sinusoidal oscillations that track the optimum.



(b) Too low: no tracking of the optimum.

(c) Too high: no oscillations.

Figure 2.13: Comparison of the effects of the *ES* gain hyperparameter. The graphics are taken from [59].

# 3



## PREPARATION

Having introduced the tools and features that were necessary for this work, it is time to take a detailed look at the required preparation. A differentiation is made between the work presented in this thesis and the project that it belonged to. The project started in June 2022 [60].

This section includes formalities that have been covered:

- Show the conducted research to validate requirements towards both algorithms and physical properties of the beam.
- Lay out the state of the project in order to:
  - Reveal existing problems and identify solutions how to mitigate them.
  - Assess risks associated with autonomous operations.

### 3.1 Initial conditions of this thesis and previous results

---

#### 3.1 Initial conditions of this thesis and previous results

At the start of this work, the project was already ongoing and yielded mixed results [60]: a first proof-of-concept had proven successful in controlling the MTE efficiency at the desired value, as seen in Fig. 3.1. On the other hand, Fig. 3.2 shows how these experiments were not always successful.

According to the state of the project at the beginning of the presented work, the following actions were determined to improve the control of the MTE splitting [10, 61–63].

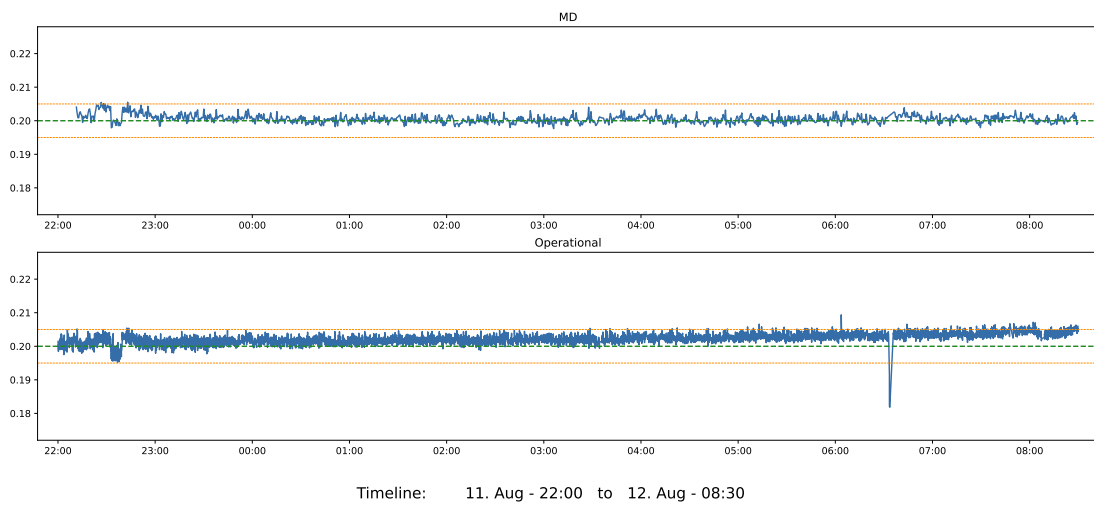


Figure 3.1: First successful MD slot in this project. The plots are taken from [59]. The operational cycle at the bottom is running as a control group. The MD cycle at the top shows how well *ES* has performed.

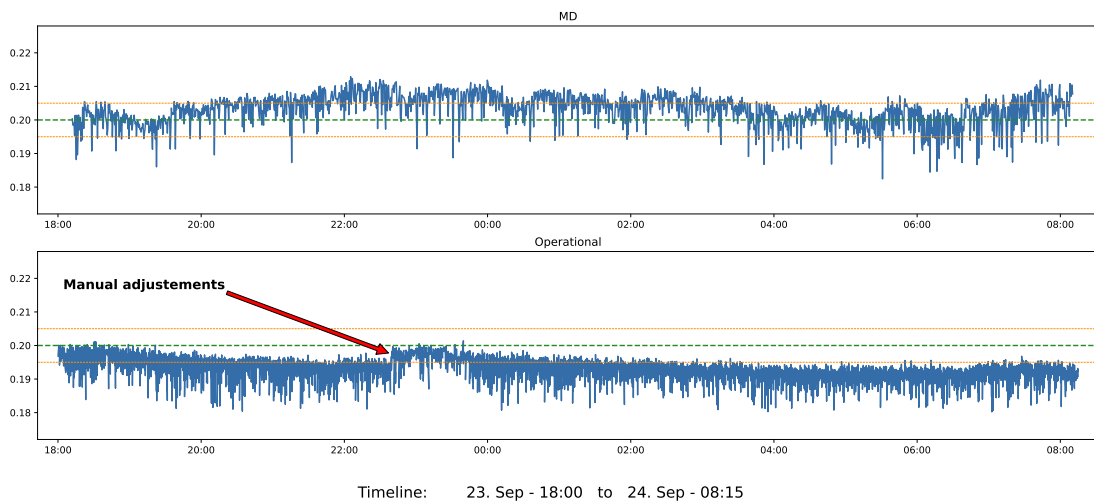


Figure 3.2: This MD slot shows, how *ES* is not always performing as desired. The plots are taken from [59]. The top plot shows the MTE efficiency under the influence of *ES*. The bottom plot is the operational cycle.

**Convex cost function** At the start of the project, the convexity of the cost function was assumed but never verified. To ensure that this fundamental property is fulfilled, this step was verified first.

**Omit the TFB gain** It is known that the TFB gain has complex implications towards the beam dynamics. This infers that the weight added to the cost function is inherently difficult to scalarise. Following the keep it short and simple (KISS) principle, it has been opted to omit the TFB gain in the first experiments of this work. This decision has been made to be able to validate the efficacy of the developed method in a bottom-up approach.

**Validate the cost function using an optimiser** To assess the accurateness of the cost function, the cost function should be working for any application of the *BOBYQA* and *ES* algorithm [61]. As the episodes of a *BOBYQA* run take considerably less time than observing its impact in the *ES* control algorithm, this property is crucial for the development time required for the cost function.

**Verify that optimisation episodes are reproducible** At the start of this work, both *COBYLA* and *BOBYQA* episodes did not provide consistent results. Consecutive episodes kept on finding different values. This property was monitored closely during the design of the cost function.

**Results of the previous experiments** Figure 3.3 shows how the MTE efficiency was distributed during the course of the experiments conducted before this work began. The median value has decreased from 0.1979 down to 0.1974. This loss in performance motivates once more the call to action presented by this work. The distribution of the experiments under the influence of the algorithm is a key indicator for the assessment of this work.

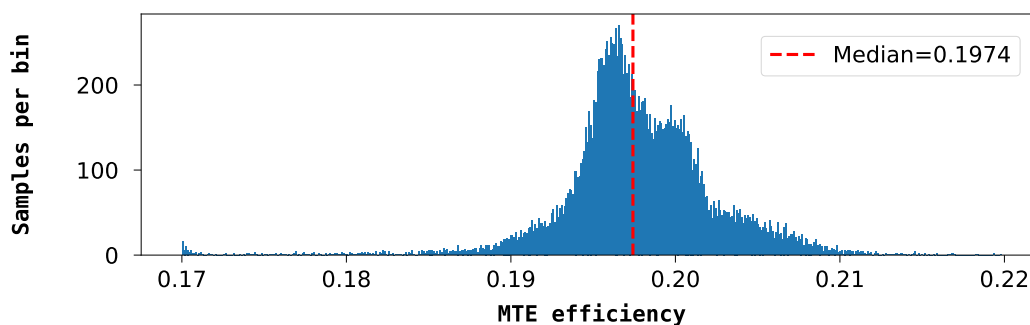


Figure 3.3: Distribution of MTE efficiency before the start of this work. Sample size: 18 464.

### 3.2 Parameter grid search

To ensure that the problem space is convex, a parameter grid search was done. For this a cartesian product of the different settings was made and then scanned over the course of an afternoon. The colour scale in the 3D plot in Fig. 3.4 shows the delta to the optimal efficiency  $n_{MTE}^{optimum} = 0.2000$  in absolute distance. It shows a clear convex function.

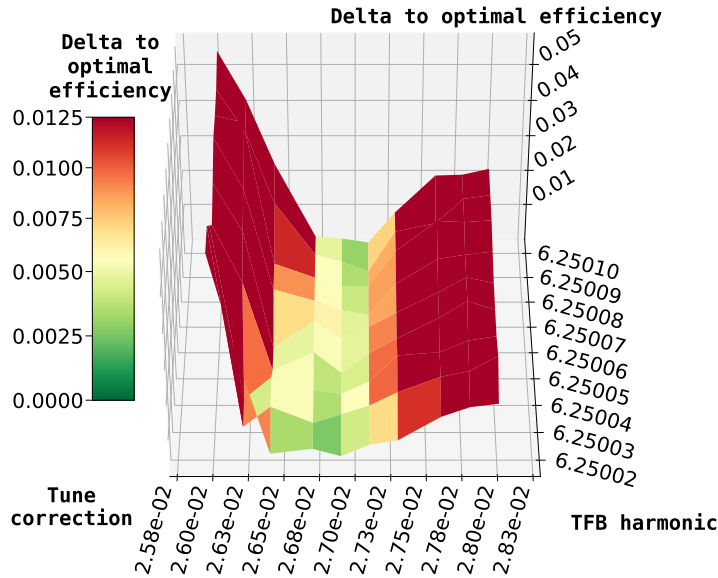


Figure 3.4: Grid search of the primary parameters used to control the MTE efficiency. Data recorded on 19 October 2022.

To mitigate the noise in the measurements, the mean value of three samples was taken for each parameter pair. As every additional sample per parameter pair substantially increases the time required for the grid search, it has been carefully chosen how many samples are effectively reducing the noise. To assess an efficient sample size, the standard deviation over a large MTE efficiency time series smoothed by different moving average windows  $n$  has been analysed, as seen in Fig. 3.5.

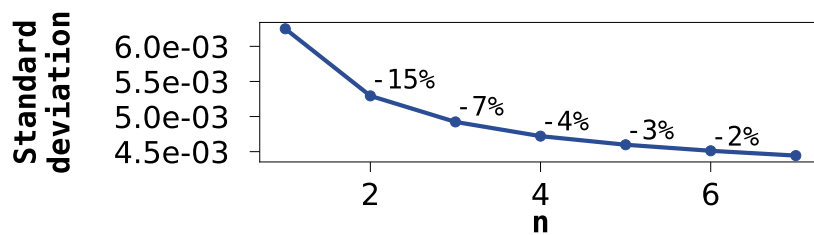


Figure 3.5: Impact of different moving average window sizes. The standard deviation of a large MTE efficiency time series was considered. The lowered fluctuation relative to the previous datapoint is annotated.



### 3.3 Problems with the existing cost function

Figures 3.6, 3.7 and 3.8 illustrate the problems of the cost function. Each figure represents one optimisation episode using *COBYLA*.

On top, the history of the relative settings of the actuators for each step during the episode is shown. In the second plot shows the evolution of the MTE efficiency as well as the objective function. Finally, the initial and final values in absolute numbers are shown.

The settings history on the one hand shows the exploration phase that has been mentioned in Section 2.5.1, these are visible in steps 1 – 3. Then, it shows how the algorithm finally approaches the minimum value of the cost function by carefully tuning the actuators. It is visible how the MTE efficiency is converging to its optimum  $n_{\text{MTE}}^{\text{optimum}} = 0.2000$ .

The problem has been that the settings were changing between each episode despite identical initial conditions. This indicates that the objective function is not finding the minimum of the convex function that has been shown in Section 3.2.

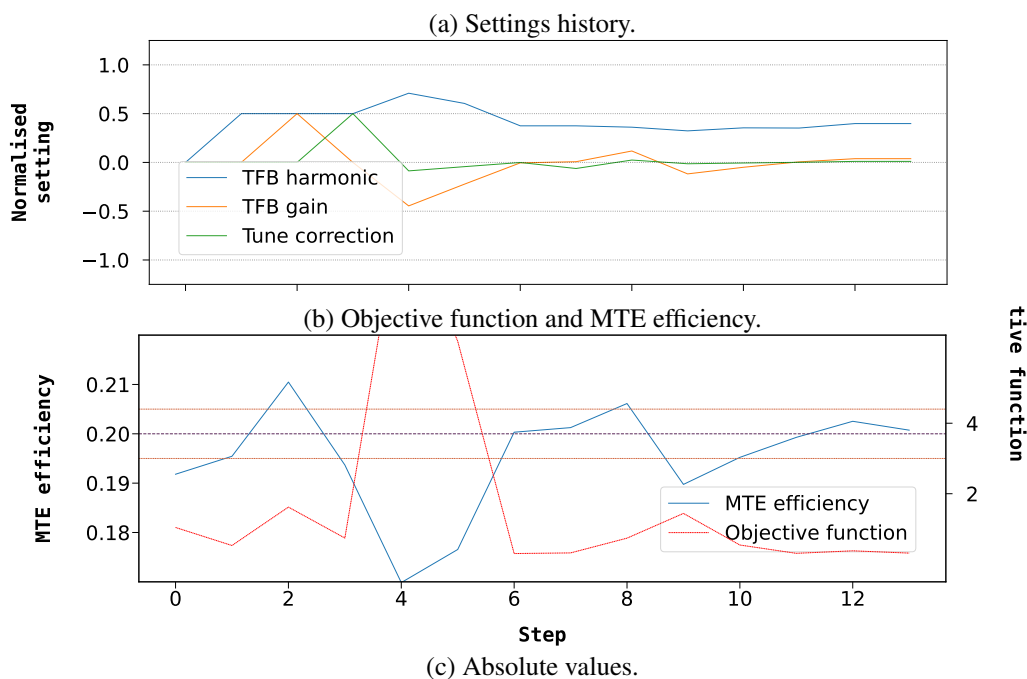
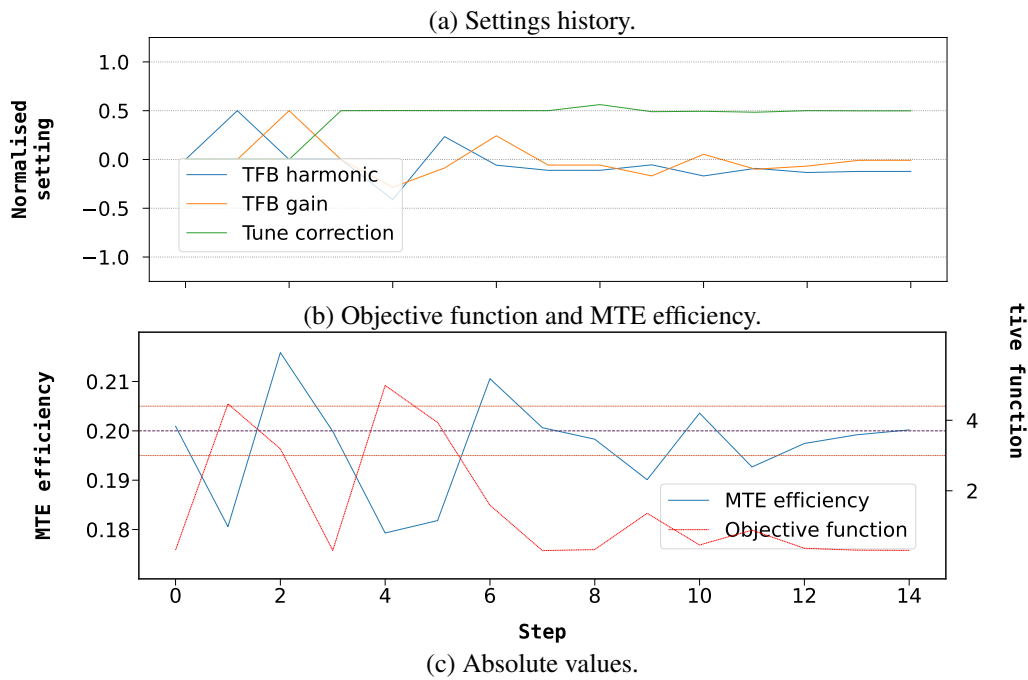


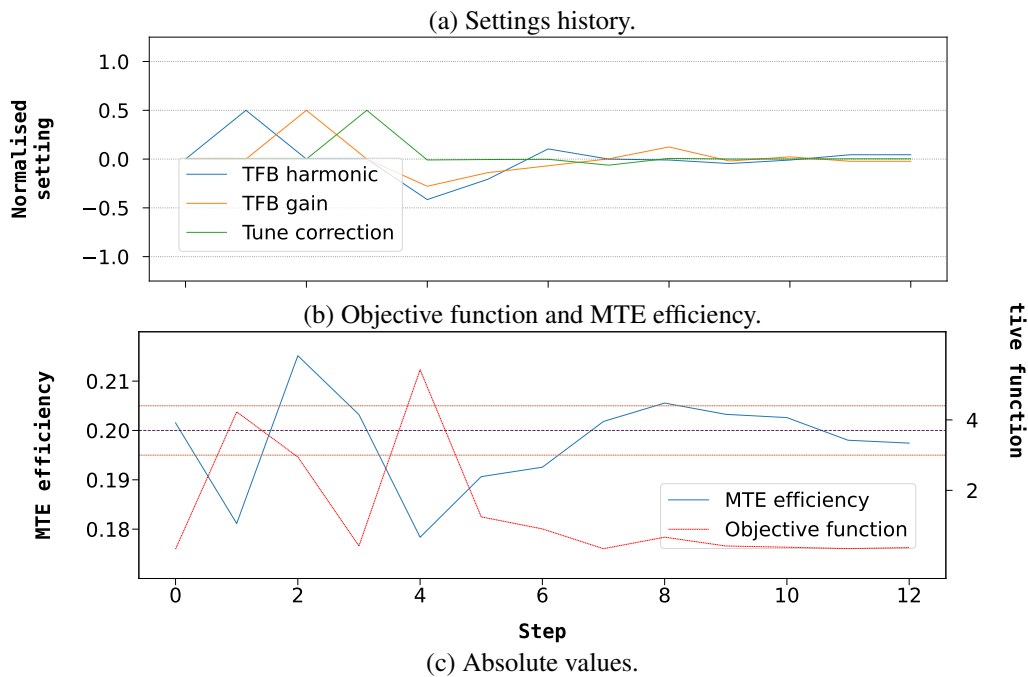
Figure 3.6: *COBYLA* example episode 1. Data recorded on 13 October 2022.

### 3.3 Problems with the existing cost function



	Tune correction	TFB harmonic	TFB gain	MTE efficiency
Initial value	0.0278	6.25021	0.0608	0.2009
Final value	0.0281	6.25017	0.0604	0.2002

Figure 3.7: *COBYLA* example episode 2. Data recorded on 13 October 2022.



	Tune correction	TFB harmonic	TFB gain	MTE efficiency
Initial value	0.0281	6.25017	0.0604	0.2015
Final value	0.0281	6.25018	0.0593	0.1974

Figure 3.8: *COBYLA* example episode 3. Showing one successful episode. The following episode yielded different results again. Data recorded on 13 October 2022.

### 3.4 Implementing safeguards

In order to design the implementation of the algorithm with a highest possible degree of autonomy, various limitations have to be taken into account. The aspects can have their origin in physics, in other hardware limitations or simply ensure that only clean data is fed into the algorithm. Therefore, the following safeguards were implemented.

**Tune** Setting the tune too high will perturb the splitting of the beam, this typically results in major beam losses. This has happened in the past and resulted in radiation alarms [60]. The reasons are twofold and can be as simple as due to software bugs or due to the algorithm behaving unexpectedly. To avoid this, an absolute threshold of the tune correction was set and warns the user that manual intervention is necessary before continuation.

**Timing for online control** Because of different reasons, it has been decided for the *ES* algorithm to only act upon one specific cycle per SC. As changes to the settings are continuously recorded to the *LSA* database, an algorithm permanently changing the settings could jeopardise the latency and therefore functionality of the database. This limitation will be relieved in the future, as transient settings which will be logged at a lower sample rate are currently under development for upcoming versions of *LSA* [64].

Additionally, in regards to minimising the external impact on the *SFTPRO* cycle, only one cycle with an identical position within the SC is considered. This is achieved by subscribing to the timing server available via *JAPC* and verifying the BP index of the cycle.

**Monitor beam intensity in TT2** To assure that the algorithm is predominantly provided with clean data, the intensity of the ejected beam is closely monitored when traversing the transfer line. At this moment, the comparison of target to actual performance of the beam is made. If the actual performance is below a certain threshold, this typically indicates a problem with the beam that the algorithm cannot address.

To avoid this corrupted data to have any impact on the performance of the algorithm, this data will simply be ignored, and the current step is skipped.

# 4



## COST FUNCTION DESIGN AND ALGORITHM TUNING

The development of the cost function for this work followed a bottom–up approach which resulted in an iterative process. This process made sure that the milestones were built upon successively and fulfil their efficacy for each individual step. As the ultimate goal is to utilise the cost function with the *Extremum Seeking* algorithm, the steps are each performed over a prolonged period of time, either over the course of the night or during a weekend. The steps are built upon each other, and the experiments are listed chronologically.

#### 4.1 Milestone 1: core of the cost function

After unsuccessful attempts presented in Section 3.3, the development process of the cost function had to begin from scratch. This time, the design was based on an approach developed at *DESY* [65]. The key idea is to incorporate a logarithmic objective [66]. In order to achieve this, the function  $C_{\text{Core}}$  shown in Eq. (1) was designed.

The MTE efficiency as function of the cost was then analysed employing different configurations. The idea was to penalise cycles where the MTE efficiency is beyond a defined, acceptable range while avoiding an overly idealistic narrow gap in order to adhere to the noisy nature of the recorded inputted data. This was achieved with the factor  $w_f$ . Figure 4.1 shows different variations of  $w_f$  considered in the process as well as the chosen factor,  $w_f = 5000$ , for the remainder of the experiments conducted in this work.

$$C_{\text{core}} = \ln(1 + w_f | n_{\text{MTE}} - n_{\text{MTE}}^{\text{optimum}} |) \quad (1)$$

Finally, the new cost function was then tested using *BOBYQA*. This time using the TFB harmonic and the tune correction, omitting the TFB gain as mentioned in Section 3.1. After carrying out repeated experiments to verify that the optimiser does find identical configurations of settings for identical initial conditions (unlike in Fig. 3.7a), it was then attempted to modify the initial values set prior to the optimisation run. The results are shown in Figs. 4.2 and 4.3.

Like Section 3.2, in order to minimise the noise in between the steps of the optimiser, *BOBYQA* was configured to take the average of three samples per step for processing.

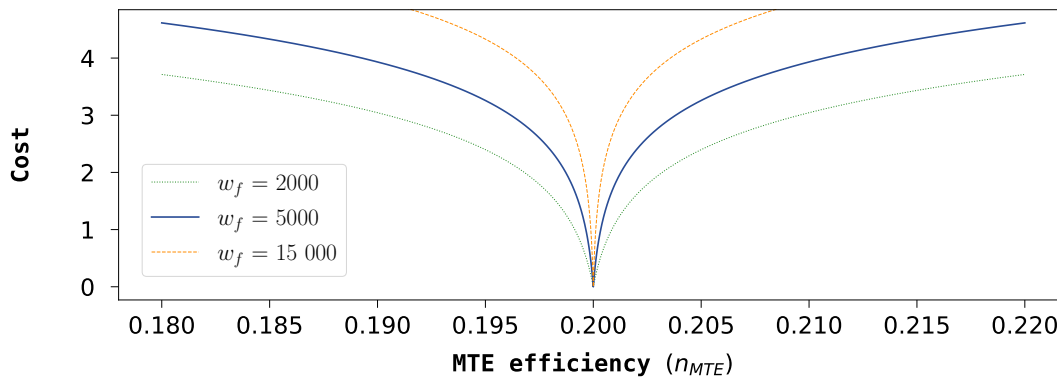


Figure 4.1: Dependency of  $C_{\text{Core}}$  on  $n_{\text{MTE}}$  and  $w_f$ .

#### 4.1 Milestone 1: core of the cost function

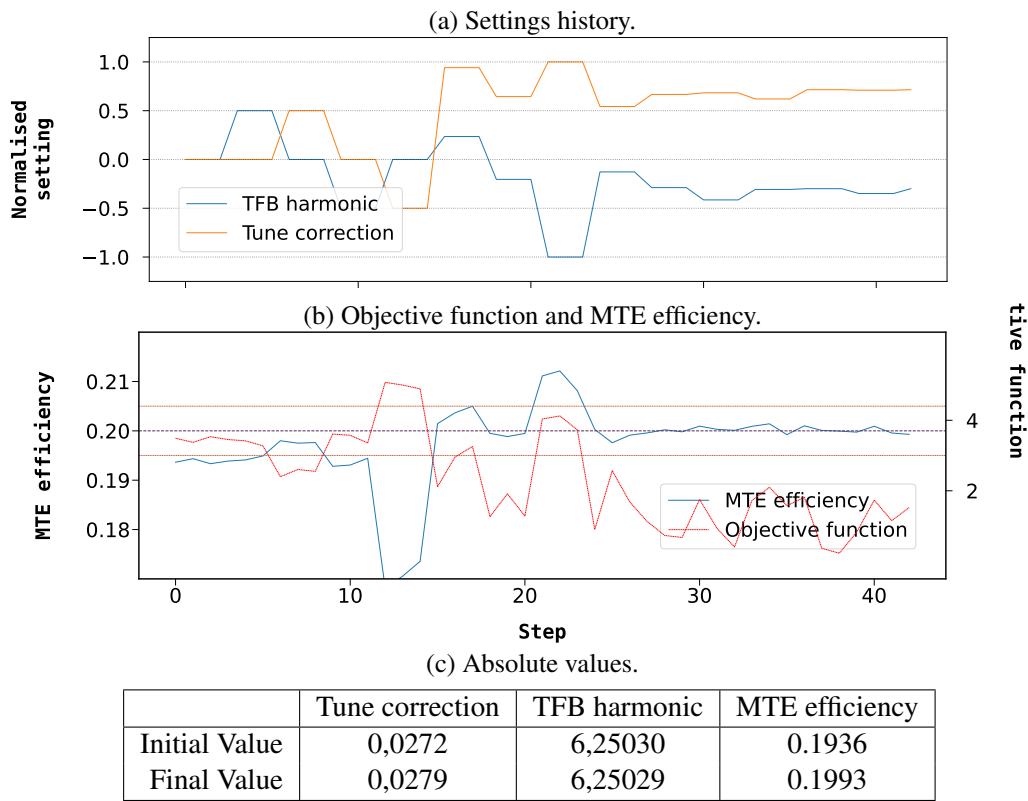


Figure 4.2: Trying out the updated cost function – *BOBYQA* example episode 1. Data recorded on 28 October 2022.

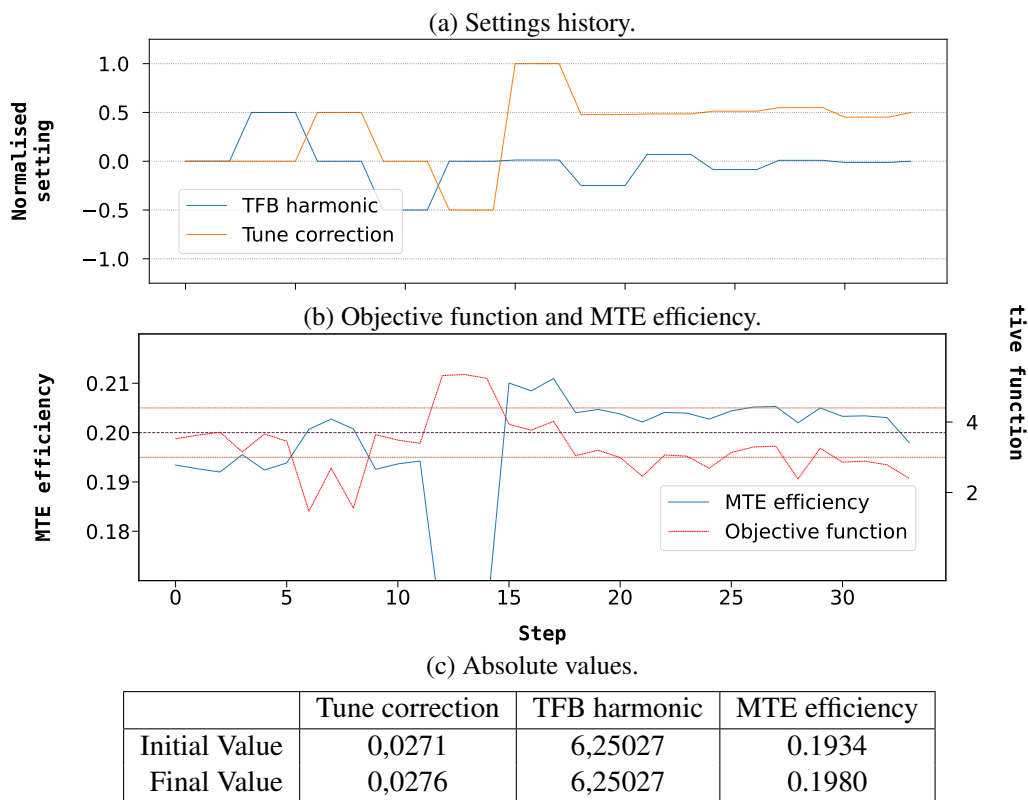


Figure 4.3: Trying out the updated cost function – *BOBYQA* example episode 2. Data recorded on 28 October 2022.

Finally, the results shown in the Figs. 4.2 and 4.3 were satisfactory in order to start an experiment using the *ES* algorithm. Figure 4.4 shows the excellent results that were achieved, both in terms of overall performance as well as its resilience against external perturbations.

Two periods without beam are also shown in Fig. 4.4. The first one occurred on 29 October around midnight for about an hour. With the *SC* not being modified in any significant manner, *ES* was perfectly capable to recover from it and continue right where it left off.

The next break, starting at around 3:00 on 29 October and lasting for about 3 hours, looks considerably more eventful. A significant shift is visible in the trend of the curve. What is remarkable is that after an hour, the curve started to shift back to its optimal value again. Similar shifts are then also observed within the same timeline at different time of days. Most notably, the other shifts did not have any interruptions taking place imminently before their occurrences.

These other shifts took place on 30 October, again around midnight, then at noon on the same day and the following day, 31 October again around midnight. This experiment was a major success and validated the currently adopted methodology.

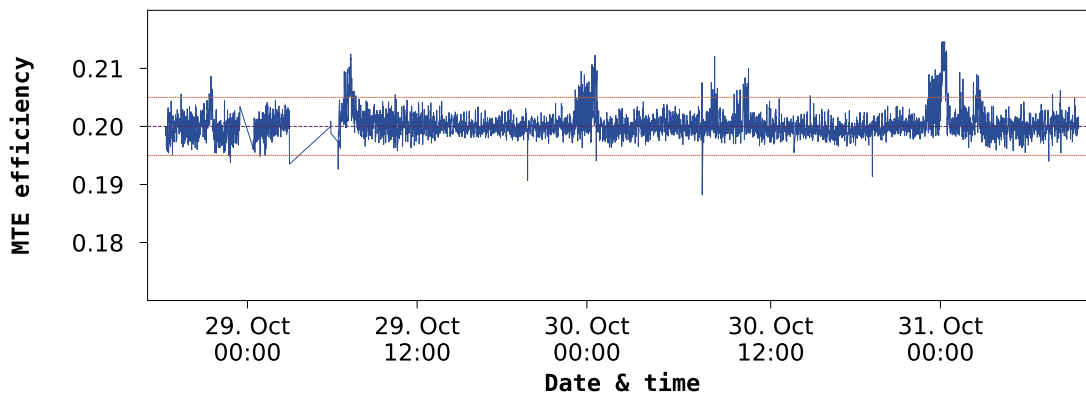


Figure 4.4: MTE efficiency evolution influenced by *ES* over the course of the weekend. Data recorded from 29 October to 31 October 2022.

## 4.2 Milestone 2: cost function weight for the TFB gain

After a successful experiment using the TFB harmonic and the tune as actuators, the next step was to incorporate the gain of the TFB by designing an appropriate weight  $W_{\text{TFB}}$  for the cost function.

It is desirable to maintain the TFB gain as low as possible in order to minimise the transverse emittance of the beam [10] but setting the TFB gain below a certain threshold will decrease the MTE efficiency. Additionally, the algorithm must be discouraged to increase the TFB gain disproportionately.

To reflect these properties in the design of  $W_{\text{TFB}}$ , it was chosen to define a realistic minimum  $\text{opt}$  for the TFB gain setting. The idea of  $\text{opt}$  is to discourage TFB gain settings lower than  $\text{opt}$ , as lowering it should not sacrifice the performance of the MTE efficiency. To prevent the algorithm to unnecessarily correct the performance of the MTE efficiency by increasing the TFB gain, the cost of increasing the TFB gain increases exponentially whenever set higher than  $\text{opt}$ . To control the steepness of the exponential slope beyond  $\text{opt}$ ,  $b$  was introduced as an additional factor.

These design features were then incorporated into  $W_{\text{TFB}}$  shown in Eq. (2).

$$W_{\text{TFB}} = e^{((\text{tfb\_gain\_setting} - \text{opt}) \cdot b)} \quad (2)$$

The results of different choices of  $b$  are shown in Fig. 4.5.  $b = 16$  and  $\text{opt} = 0.16$  were chosen empirically for  $W_{\text{TFB}}$ .  $\text{opt}$  is indicated by the grey lines.

The cost function featuring the newly designed weight was then first validated using the *BOBYQA* algorithm. The results of these experiments are shown in Fig. 4.6 and Fig. 4.7.

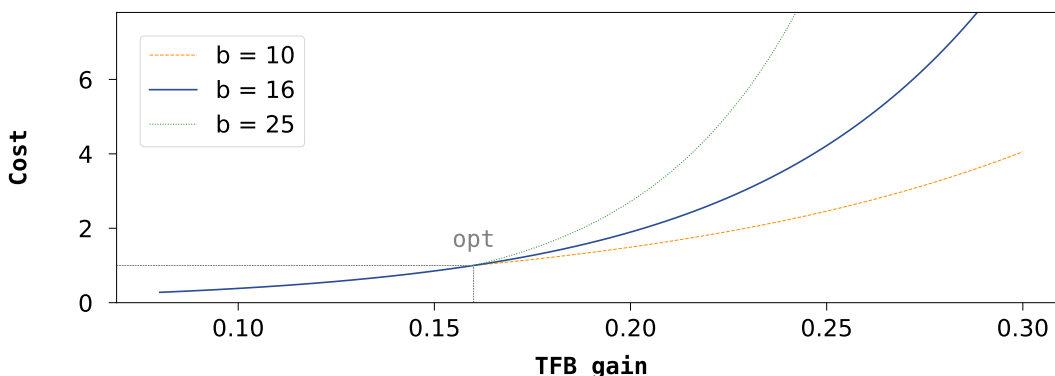
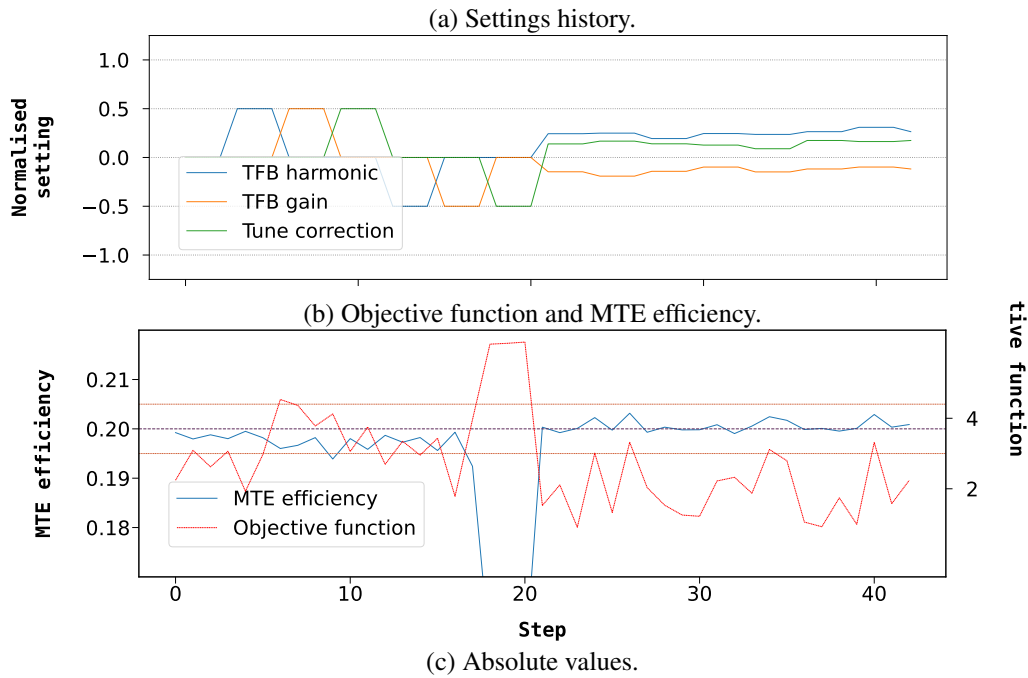


Figure 4.5: Dependency of the cost function on the TFB gain setting and chosen parameter  $b$ .

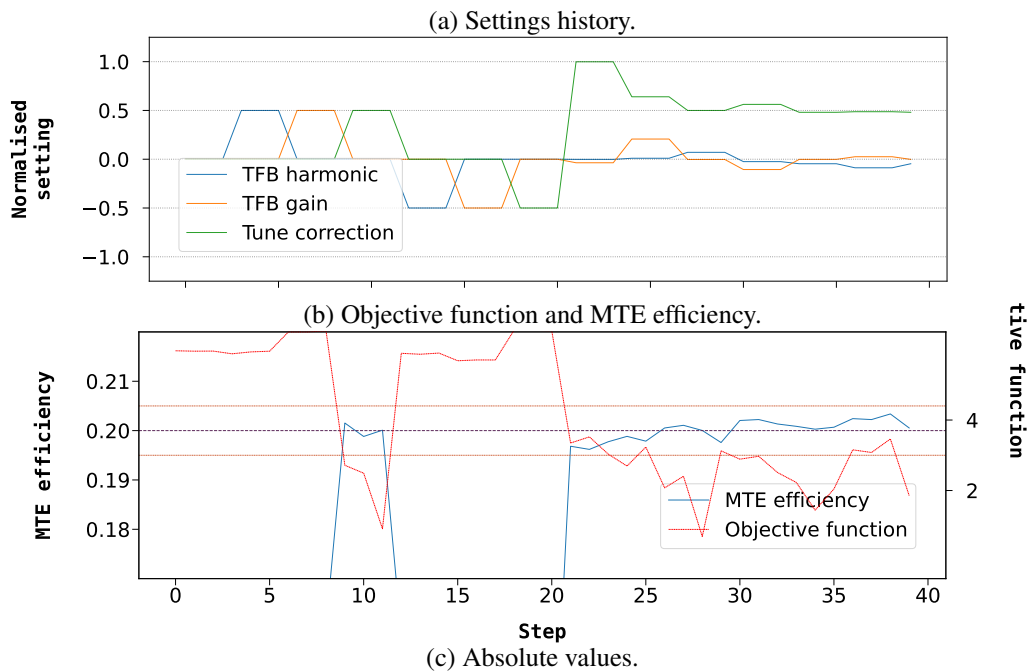




(c) Absolute values.

	Tune correction	TFB harmonic	TFB gain	MTE efficiency
Initial Value	0,0273	6,25033	0.1400	0.1992
Final Value	0,0274	6,25034	0.1306	0.2009

Figure 4.6: Trying out the updated cost function – *BOBYQA* example episode 1. Data recorded on 31 October 2022.



(c) Absolute values.

	Tune correction	TFB harmonic	TFB gain	MTE efficiency
Initial Value	0,0268	6,25034	0.1306	0.1555
Final Value	0,0273	6,25034	0.1305	0.2005

Figure 4.7: Trying out the updated cost function – *BOBYQA* example episode 2. Data recorded on 31 October 2022.

## 4.2 Milestone 2: cost function weight for the TFB gain

---

After being satisfied with the results from the optimiser, it was then time to launch the changes to the cost function again using *ES*. The evolutions of the MTE efficiency as well as the settings resulting from the actuators are shown in Fig. 4.8.

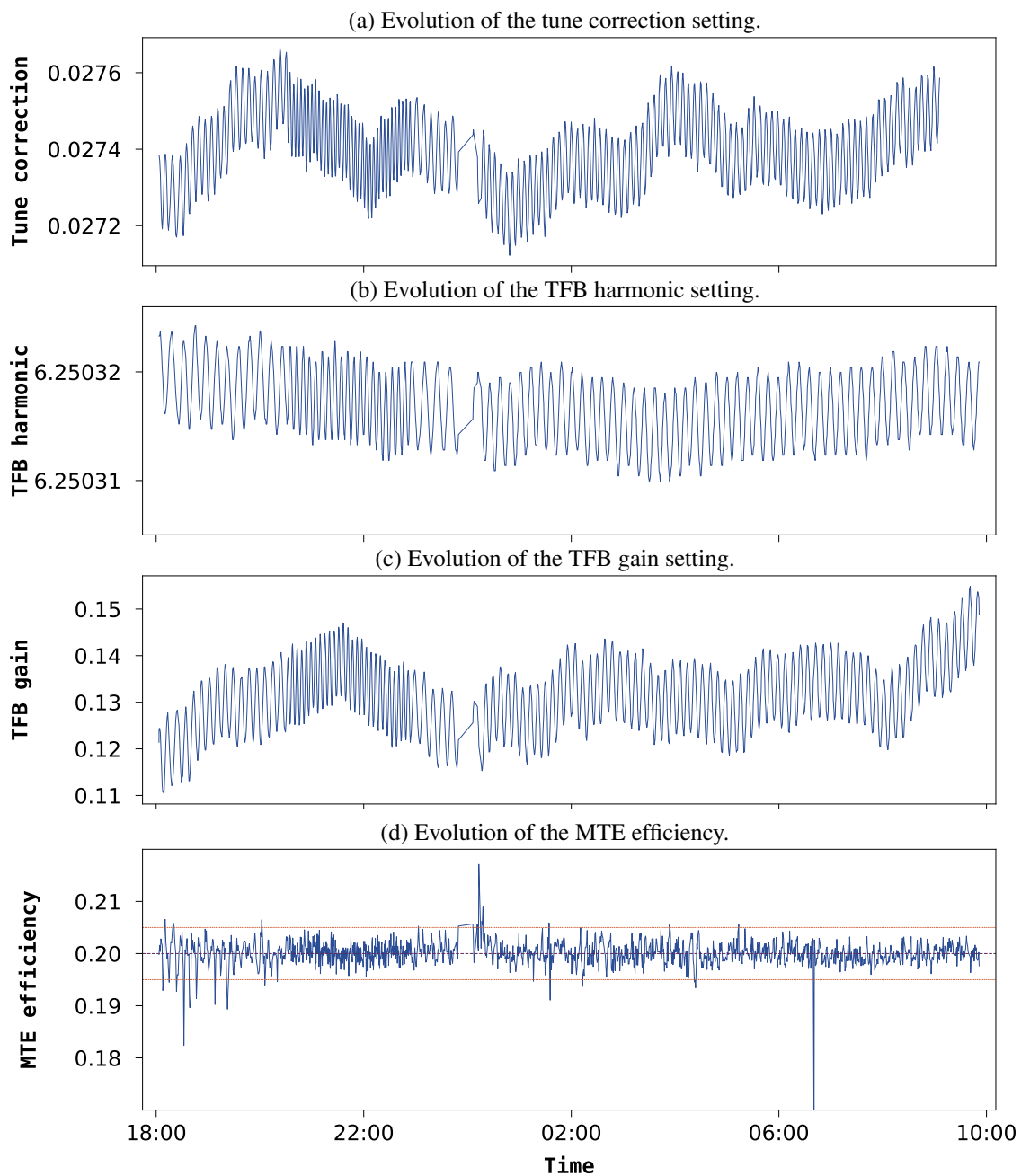


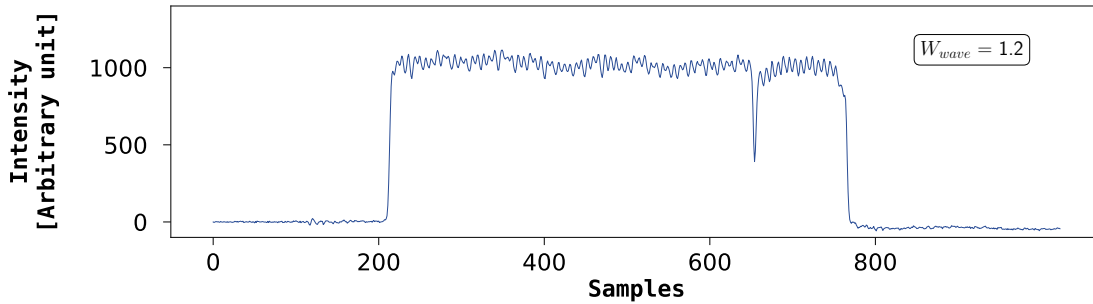
Figure 4.8: MTE efficiency evolution influenced by *ES* over the course of the night. Data recorded on 31 October 2022.

### 4.3 Milestone 3: cost function weight for the spill waveform

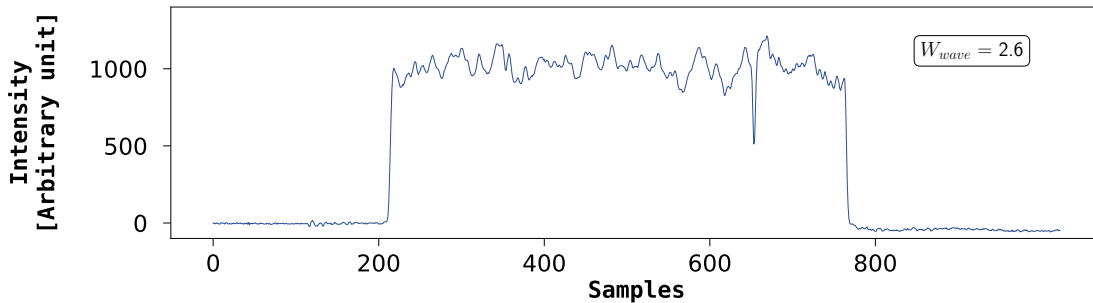
After successful integrations of the first two goals of the algorithm, it is time to approach the design of the weight of the waveform quality of the spill  $W_{\text{wave}}$  for the cost function. The shape of the spill plays a crucial role for the fixed target experiments. Ideally, the waveform of the spill looks like a square wave. Figure 4.9a shows a spill as it is commonly observed after being ejected from the *PS*. The plateau of this waveform is about as straight as it will realistically become.

Since the spill is measured using multiple samples, extracting a scalar suited for the cost function is challenging. To quantify this metric, various functions have been applied to a collection of random spill samples. The metric has then been compared to the waveform of the spill and its suitability was assessed manually. After experimenting with multiple functions and comparing various metrics empirically, the following weight, as presented in Eq. (3) was adopted where  $x$  is the standard deviation taken from the spill measurement<sup>7</sup>. The values of the weight in accord to its waveform are shown in Fig. 4.9.

$$W_{\text{wave}} = (10^{0.25x} - 10) - 1 \quad (3)$$



(a) Example of the weight added for a beam with good spill quality.



(b) Example of the weight added for a beam with bad spill quality.

Figure 4.9: Developing a metric to quantify the spill quality.

<sup>7</sup>In order to not overstate this example, this explanation was abstracted: the signals resulting in the shown plots are postprocessed to include baseline adjustments for a more uniform representation [67]. The value used to determine  $x$  originates from the raw data as the results have shown better conformity in the testing. The design principle remains unchanged.

### 4.3 Milestone 3: cost function weight for the spill waveform

---

**Testing** After designing  $W_{wave}$ , it is time to test the results to validate its utility. As in previous experiments, the *BOBYQA* algorithm was used in this process. The outcome looks excellent. The before and after comparison of the spill are shown in Fig. 4.10.

While the spill in Fig. 4.10a exhibits poor performance, the MTE efficiency of this transfer is 0.2035. This is due to the initial settings being set by the previous experiments conducted in section 4.4. At this time, the cost function that *ES* was using uniquely targeted the performance of the MTE efficiency regardless of its implications on the waveform of the spill.

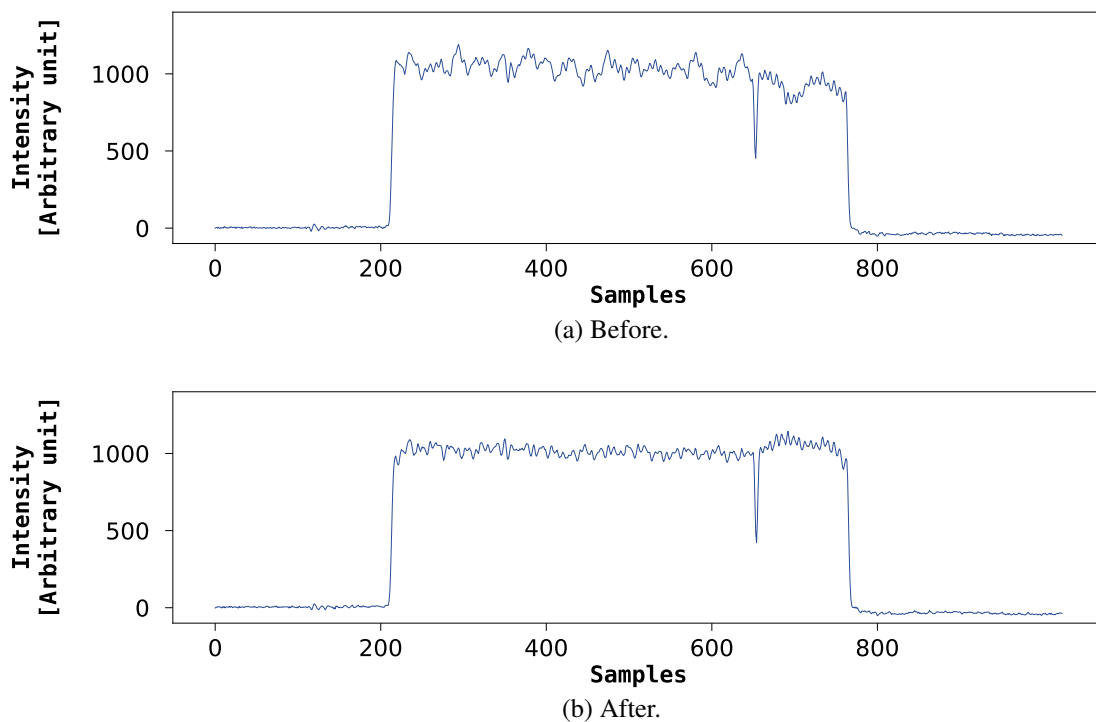


Figure 4.10: Before and after comparison of the waveform of the spill after a *BOBYQA* optimisation episode. Data recorded on 04 November 2022.

## 4.4 Hyperparameter tuning

After designing the cost function, it is now time to tune the settings of the *ES* algorithm itself. The changes were made to the hyperparameter, which defines the oscillation amplitude of the actuators. It was decreased to 0.06 from its default value of 0.1. A larger oscillation amplitude implies fluctuations induced by *ES* itself. Therefore, this hyperparameter should be kept to a minimum while maintaining an expressive oscillation required by *ES*.

Figure 4.11 shows how this experiment was another success in demonstrating the performance of the *ES* algorithm. No loss in performance was observed after this modification.

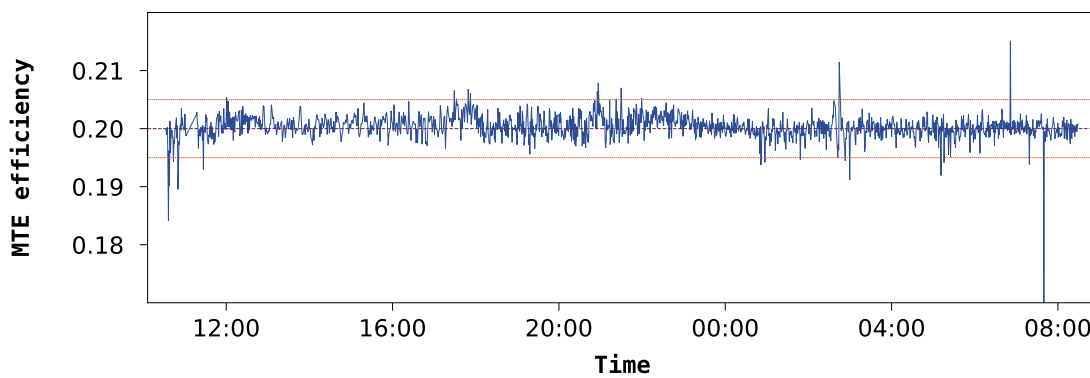


Figure 4.11: MTE efficiency evolution influenced by *ES* over the course of the night. Data recorded on 03 November 2022.

## 4.5 Final demonstration

After the work presented in Section 4.3, various experiments were conducted. These will become relevant for the final section concerning the outlook of this work. Before the shutdown of the machines, a final demonstration to verify the findings of this work was carried out on 24 November 2022. This was done in order to collect further evidence of the capabilities of the *ES* algorithm. Additionally, it ensured that the algorithm remains functional after various changes made to the environment of the accelerator in the final days before the YETS.

The evolution of the MTE efficiency is presented in Fig. 4.12. Generally, the performance is solid, but runaways are visible between 03:00 and 05:00. A clear shift in the recorded MTE efficiency becomes visible again. Subsequently, the timeframe was inspected using the *Supercycle State Tracker (SST)*, presented in Section 5.3, and revealed a substantial change in the SC at approximately 03:12. This change was then reverted to its previous configuration at around 04:45. To substantiate this claim even further, the configuration that was present before 03:12 was active for 14 SCs between 03:45 and 04:00. These changes, in particular the short-lived change between 03:45 and 04:00, correspond exactly to the shifts in MTE efficiency that are visible in the time series.

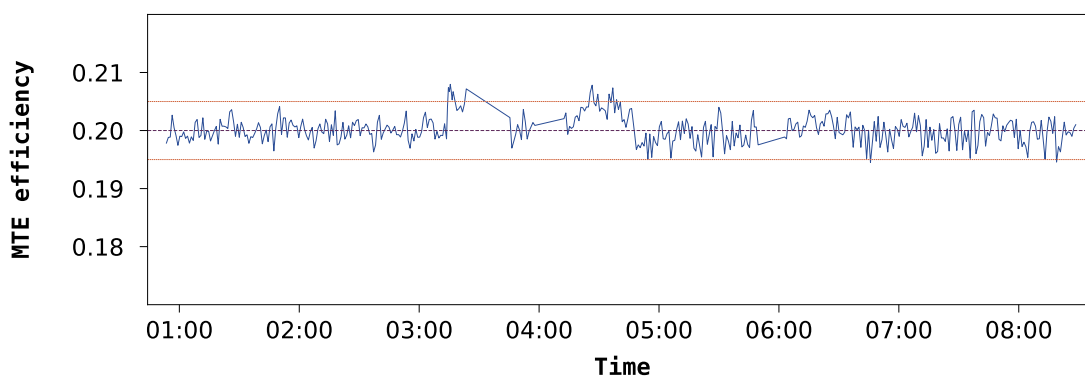


Figure 4.12: MTE efficiency evolution influenced by *ES* over the course of the night. Data recorded on 24 November 2022.

# 5

---

## CONCLUSION

Following the journey of the experiments carried out previously, this section will be dedicated to the resulting observations made during the development.

In particular, this section will:

- Take a detailed look at the encountered problems and how they were resolved.
- Demonstrate specific problematic scenarios.
- Highlight the final performance of the MTE efficiency distribution.

## 5.1 External perturbations

**First observation** Figure 5.1, when the *ES* algorithm did not manage to control the MTE splitting properly. During the beginning of this period, it was working fine amidst the occasional spikes. Occasional spikes appeared between 02:00 and 10:00 and were understood to be solely linked to *Linac4* problems [68] and therefore reached the *PS* in an erroneous condition. The safeguards mentioned in Section 3.4 were working as intended and intercepted the value before feeding it into the active algorithm.

But starting from 10:00, external perturbations appeared that shifted the efficiency upwards. Perturbations in general are expected this day as Wednesday marks the day of the week that is dedicated to carrying out MD tests. From 08:00 to 18:00, the physics programme is set to low priority in favour of tests.

The source of the perturbations on that day will likely never be fully understood. Modifications in the SC are expected to be at the source as they changed the magnetic behaviour of the accelerator [69].

As a conclusion, the results will not be considered for a final conclusion on the performance of the algorithm overall. But attempts to understand what happened on this day were made, nonetheless. The observations made attracted the attention on certain correlations with the SC, which will be analysed in greater detail at a later point in this work.

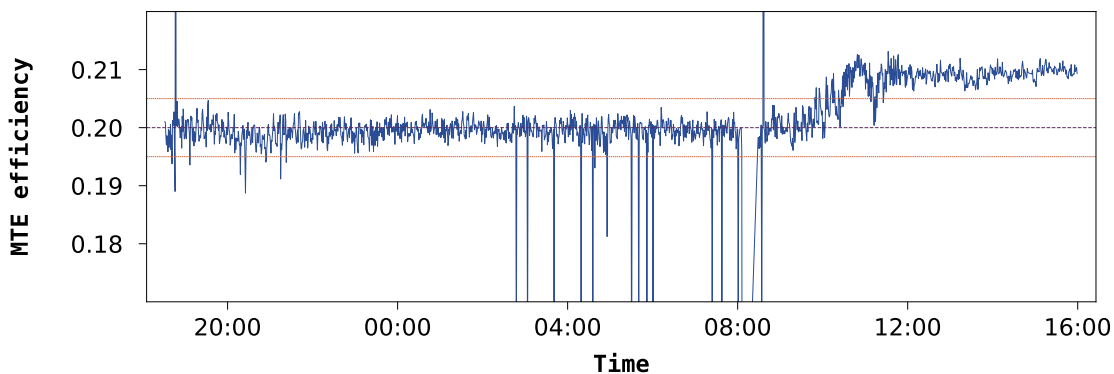


Figure 5.1: An external perturbation caused a significant drift of the efficiency towards the end of the observation period. Data recorded from 01 November to 02 November 2022.



**Behaviour of the algorithm** Figure 5.2a, shows the safeguard presented in Section 3.4 in action and proving its effectiveness by blocking the tune correction setting to be set any higher. The evolution after 10:00 shows no tune correction oscillation as result of the defined threshold.

In particular the time between midnight and 6:00 demonstrates well what happens when the external perturbations become too large for the algorithm to handle. *ES* then attempts to modify its actuators, but the modification has no beneficial impact on the performance. What happens next then becomes unpredictable and can result in catastrophic failures such as an ever-increasing tune.

Additionally, the changes at around 8:00 demonstrate the seemingly arbitrary settings chosen by the algorithm. This time, *ES* attempts to modify the gain in order to minimise the loss, also of no avail.

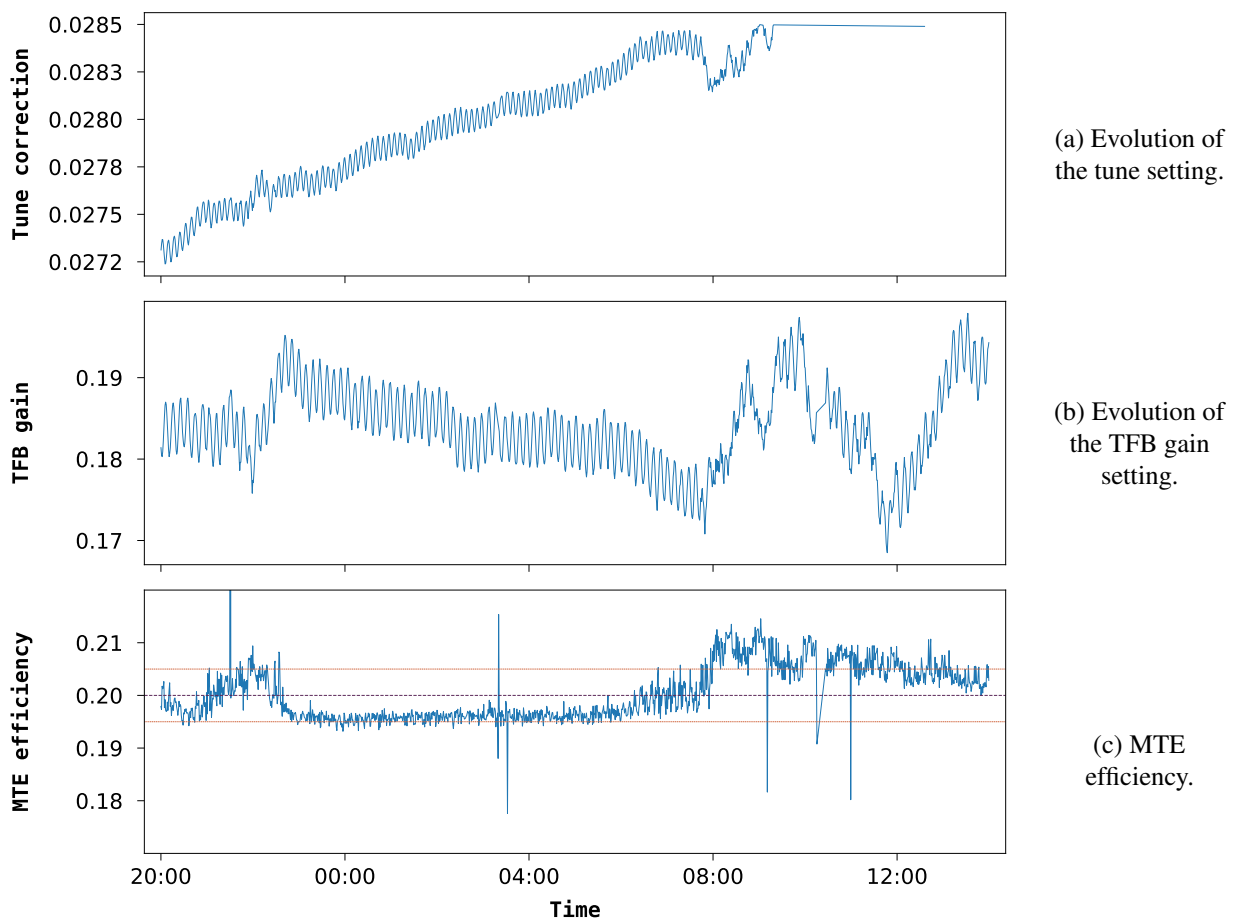


Figure 5.2: Example of the *ES* behaving unexpectedly under the influence of external perturbations. Data recorded on 04 November 2022.

## 5.2 Supercycle dependency

The idea that perturbations occur based on certain configurations of SCs has been known previously. In fact, the MTE cycle already relishes special care during its planning regarding its position in the SC because of its sensitiveness [10].

With this feature in mind, the analysis of what happened after the particularly chaotic experiments as presented in Sections 4.3 and 5.1 has been targeted towards the state of the supercycle. To illustrate this, a curated timeframe taken from Section 5.1 is now considered and a specific correlation, illustrated in Fig. 5.3 was found.

Following clues given by the presence of this cycle, this same analysis has been done regarding the various experiments that were conducted during this work. Consequently, a correlation was found amongst most anomalies that were observed during the MTE efficiency evolution.

No physical explanation for the *LHC* cycle impacting the MTE splitting of the SFTPRO cycle could be identified with the experts of the field, especially as the *LHC* and SFTPRO cycles are played several seconds apart. The consensus was reached instead to further investigate the configurations of the SC whenever an *LHC* cycle was present.

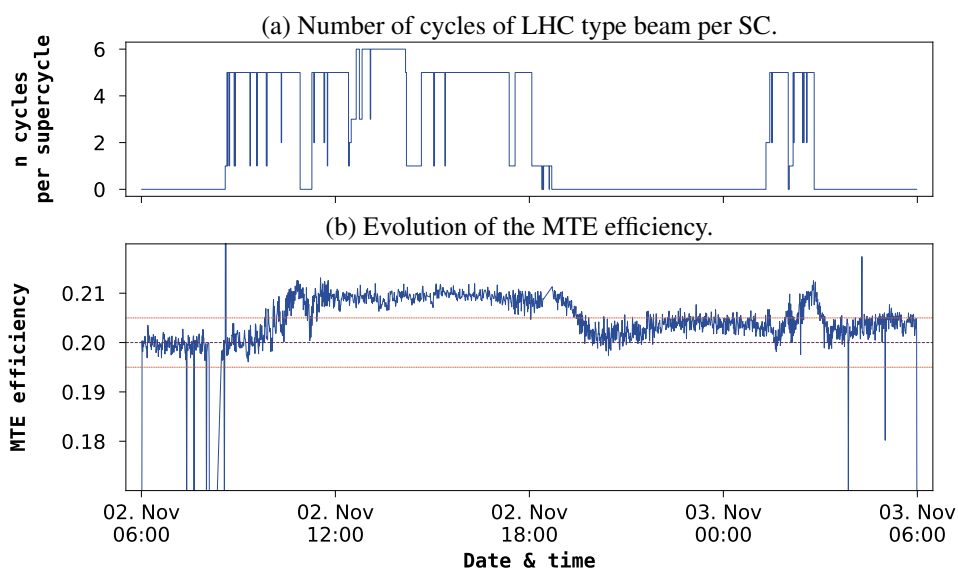


Figure 5.3: Evidence about the SC dependency of the MTE splitting.  
Data recorded on 02 November 2022.

### 5.3 SST – Supercycle State Tracker

The time series presented in the previous Section 5.2 kicked off the need to closer inspect the SC state. Generally, the analysis of the SC has proven difficult because of the abundance of categorical data. Hence, the following tool to visualise the SC configurations has been developed: the *SST*.

The *SST* has been an important tool to find evidence in regards to problematic SC configurations. An extract of the *SST* is shown in Fig. 5.4.

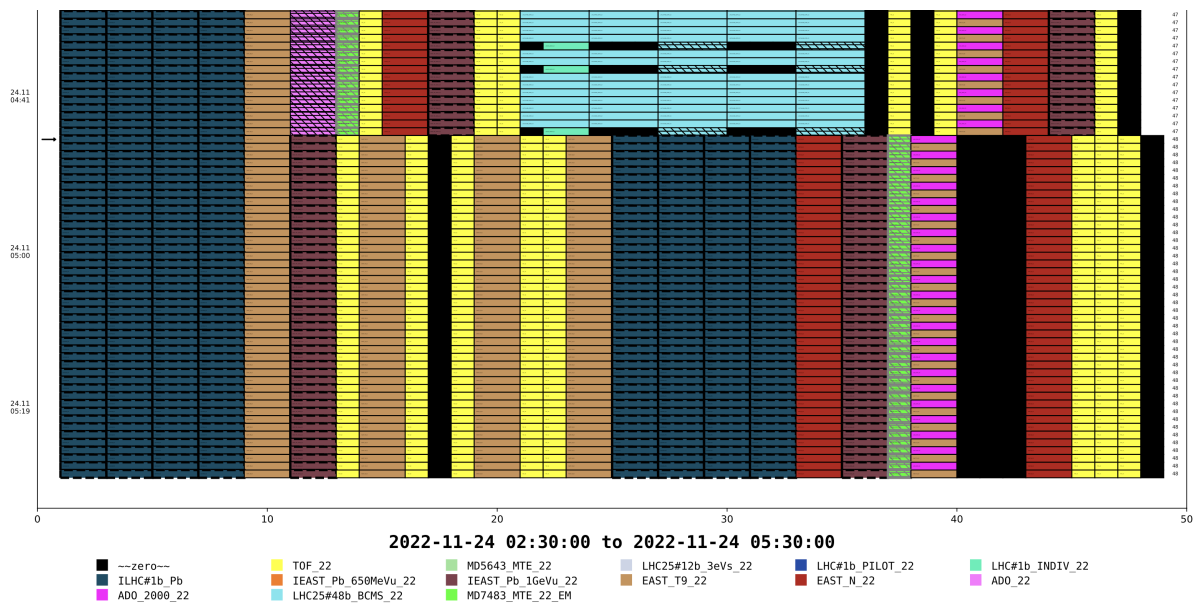


Figure 5.4: Extract of an *SST* page. Full examples are found in the appendix.

**Idea** Each SC is represented by a dedicated row. Each cycle is represented by a rectangle. The width of the rectangle varies in function of the duration of the cycle in BP. The position of the cycles increases from left to right in chronological order. The SCs are arranged in chronological order starting from the top. This way the cycles can be read intuitively in the same way as a book.

The cycles are then distinguished by a dedicated colour, which is explained by the legend in the bottom of the page. Assigning the colour has proven quite difficult for the human eye to discriminate the distinct cycles. Therefore, matching colour palettes was designed according to the *Colorgorical palettes* presented in [70].

Additional features to enhance the perceived information have been added:

- An arrow on the left-hand side that indicates an update of the configured SC.
- A counter of the current SC length on the right-hand side of each row.
- An  $x$ -axis like scale on the bottom of the page, indicating the current BP number.
- Grey rectangle borders whenever a cycle is an MD cycle.
- Hatched rectangles whenever the beam has been sent to a dump.

Since the (vectorised) output is designed to be viewed on a digital medium like a computer or tablet, tiny text notes were added within the rectangles of each cycle spelling the name of the cycle. This has proven useful to quickly disambiguate any possible conflicts from the sometimes hardly discriminable colour.

The representation is finally rendered and can be viewed on a single *DIN A4* page. During testing, rendering a timeframe of 3 hours proved feasible without compromising readability. The height and width of the rectangles are not fixed as the representation can vary, depending on the SCs that are represented in the given timeframe. Sometimes, the SC is longer, which results in taller, narrower rectangles and vice versa.

## 5.4 Hypothesis concerning the source of perturbations

The performance benefits attained thanks to *ES* cannot be tolerated at all costs. Predominantly optimal performance is not acceptable if the trade-off implies occasional loss of control as seen in Section 5.1. Getting behind the root causes of the problems and understanding how to avoid them was an extensive part of this work. Substantial efforts were made in finding patterns of different SC configurations, comparable to what was presented in Section 5.2.

Observations based on the *SST* led to inspect the MTE efficiency in function of the two preceding cycles of the MD SFTPRO cycle. The results of this effort are shown in Fig. 5.5. The distributions are annotated with the following information: their *LSA* context name, the lead time that it was preceding the inspected MD SFTPRO cycle and their sample size.

As the *zero* cycle is effectively an idle cycle within the SC, its random distribution, no matter its lead time, is to be expected. Subsequently, the most eye-catching configuration originates from the *EAST\_T8\_22* cycle with a lead time of 2 cycles. The distribution of this configuration, followed by a *zero* cycle, has been overlapped in orange colour. This highlights how deteriorating this configuration has been towards the performance of the MTE efficiency.

These observations suggest to meticulously monitor the state of the SC while *ES* is running. The impact of this highlighted SC configuration will be verified once the *YETS* is over.

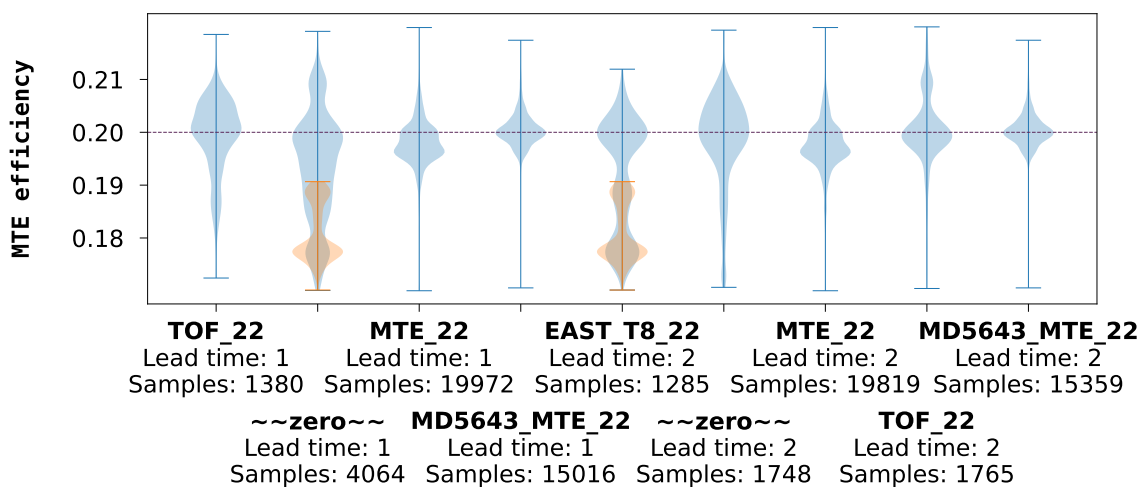


Figure 5.5: MTE efficiency in dependency of the preceding cycles to identify problematic SC configurations. The orange overlay shows the specific configuration of *EAST\_T8\_22* and *zero* cycle preceding the MD cycle. The lead time is indicated in cycles.

## 5.5 Retrospective & final comparison

The thorough outcome of the MD development is discussed in this section. The distribution shown in Fig 5.6 consists of all experiments conducted, including the ones that predate this work. The data has been coarsely filtered on outliers, 786 in total, or 1.80%, which would have obstructed the histogram. After filtering, 42 788 samples are considered. The ratio of outliers from the MD cycle corresponds roughly to the ratio of outliers from the operational cycle, which equals 1.60%.

Despite the data which makes up the distribution being influenced by a total of 82 completed optimisation episodes using *COBYLA* or *BOBYQA*, the median value in this data set has increased to 0.1990. This demonstrates a notable improvement compared to the operational data that was presented in Section 1.2. Upon inspection of the distribution, it can be characterised by three peaks that are visible around 0.1780, 0.1960 and 0.2000. These peaks have different origins:

- Peak at 0.1960: originates from the data presented in Section 3.1.
- Peak at 0.1780: originates from the SC configuration that has been highlighted in Section 5.4.
- Peak at 0.2000: the benchmark for the MTE efficiency. The success from this characteristic is now elaborated in a final comparison.

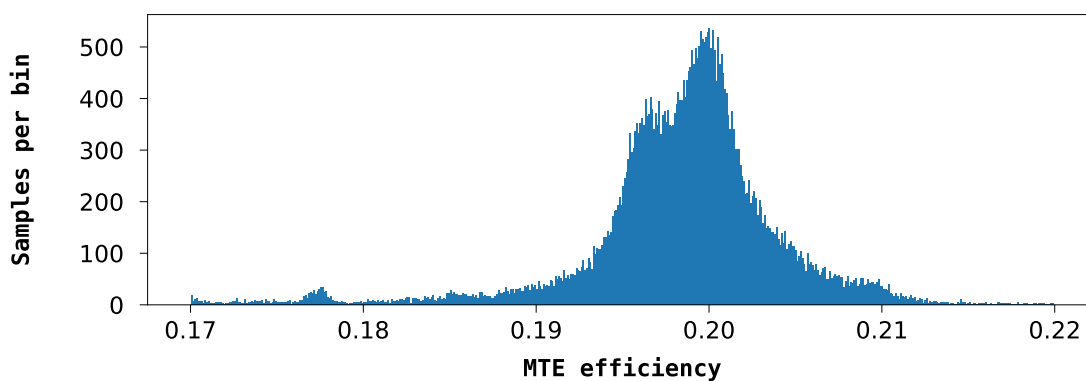


Figure 5.6: Distribution of the MTE efficiency of every single SFTPRO MD sample.

**Final comparison** Finally, to assess the achievements of this work, the distributions of various MTE efficiency data sets at the end of 2022 are considered in Fig. 5.7. The optimal value is visualised by the green dotted line at 0.20. The range of acceptance, as described in Section 1.2, is delimited by the two orange dotted lines.

The leftmost distribution, titled “Operational”, has already been shown in Fig. 1.3. The data was filtered to ensure a fair comparison between the distributions. In this plot, it becomes visible how far off the centre of the distribution is located in regards to the ideal MTE efficiency.

Next in line is the “Project” distribution that mentioned earlier in Section 3.1. It has been added as immediate comparison.

Finally, the “Work” distribution shows the distribution that highlights the results from this work. Only the samples where *ES* was applied to control the MTE splitting and where the MD SFTPRO cycles were preceded with two other SFTPRO cycles are considered. The success of this work is highlighted in the graph: the distribution is perfectly centred around the benchmark line. Indeed, the median value of this distribution is 0.2001.

To further put the achievement into numbers, consider the share of the samples that lies within the range of acceptance. This share amounts to 70.5% for the “Operational” data set. For the “Work” distribution, this share has increased by a total of 19.5 percentage points, to an outstanding value of 90.0%.

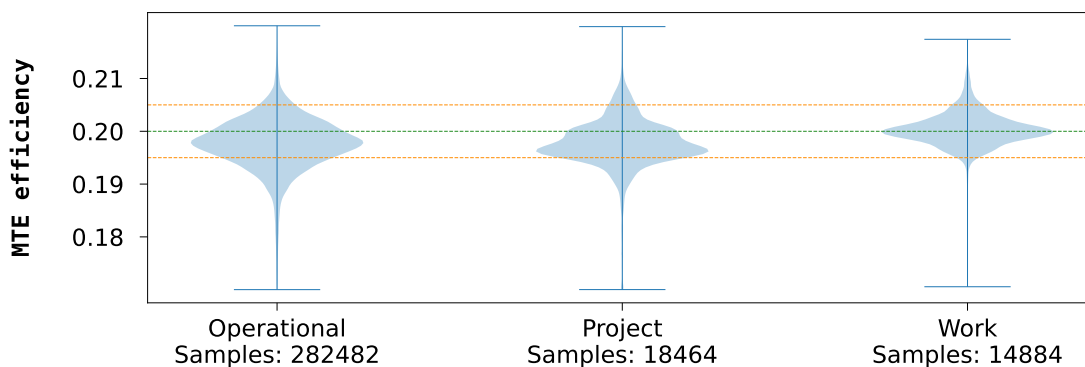


Figure 5.7: Comparison of operational and MD MTE efficiency distributions.

# 6



## OUTLOOK

Finally, after successful demonstrations of the development, the outlook and future usage of this work can be elaborated. This will cover a novel method that is currently being developed and expand on the challenges it will face for the implementation and opportunities developed in the framework of this work.



## 6.1 Future of SFTPRO: barrier bucket

The so-called barrier bucket (BB) upgrade is a novel method for the MTE beam that is currently in development. First productive tests have been conducted in the year 2022, in parallel to the developments made during the hereby presented work [10].

While in theory the changes should not affect the cost function that has been described earlier, the experiments that were translated to the BB environment falsified this theory. The results using *BOBYQA* resulted in neither performant nor coherent settings value pairs. Consider the comparable parameter grid search in Fig. 6.1. The data was acquired employing the same methodology as presented in the earlier Section 3.2. The visible valley from the previous grid search has disappeared. Now there are various local minima with no apparent relationship between the settings value pairs.

This observation marks the end of the experiments that were actively conducted in the *PS* accelerator. Therefore, the status quo at the end of the run in 2022 is that the BB upgrade added yet another obstacle towards a successful implementation of the *ES* algorithm to control the MTE splitting. Fortunately, the upcoming Section 6.2 will enlighten the assumed root causes of the problem and even expand on potential opportunities brought by these changes.

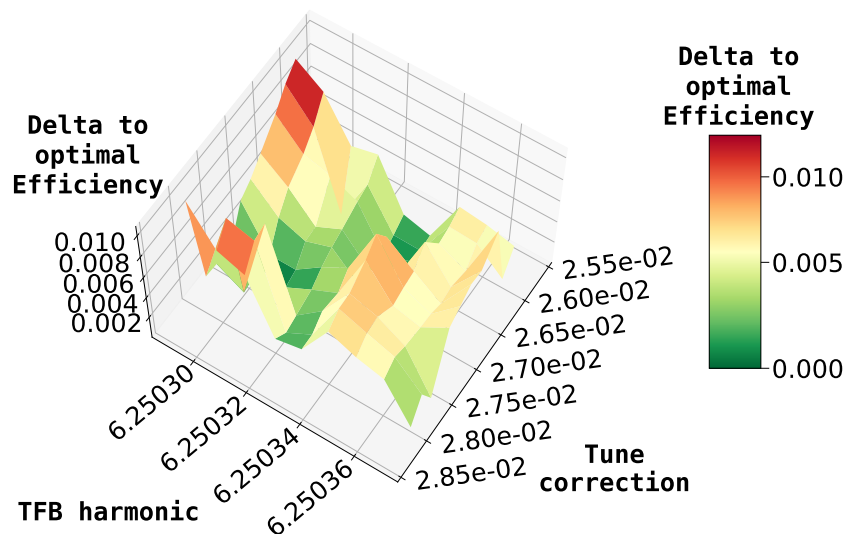


Figure 6.1: Grid search after the barrier bucket upgrades for the SFTPRO cycle.  
Data recorded on 18 November 2022.

## 6.2 Improve the observables

This section focuses on potential enhancements of the observables used for the cost function of the algorithm. These improvements were identified through insights gained during these studies as well as upcoming hardware upgrades in the *PS*.

**BGI – TFB gain vs. transverse beam size** The increase in the TFB gain has a negative impact on the emittance of the beam, as it results in a larger horizontal beam size. The horizontal beam size of the core in function of the TFB gain setting is shown in Fig. 2.2. In operations, the measurements of the transverse beam size are typically done using devices called wire scanner [72]. The drawback of a wire scanner is that the measurement can have negative effects on the beam [73].

A new device, the beam gas ionisation (BGI) monitor was developed as part of the *LIU* project [74]. The horizontal BGI monitor has been operationally stable since 2022 [75]. The beam size shown in Fig. 2.2 was determined based on Gaussian fits based on beam profiles acquired using the BGI monitor.

The BGI monitor allows to measure the transverse profile of the beam in a non-destructive way [76]. This device could be used to continuously monitor the horizontal beam size of the SFTPRO beam in the future and creates an opportunity to use the horizontal beam size as an observable in the cost function in the future.

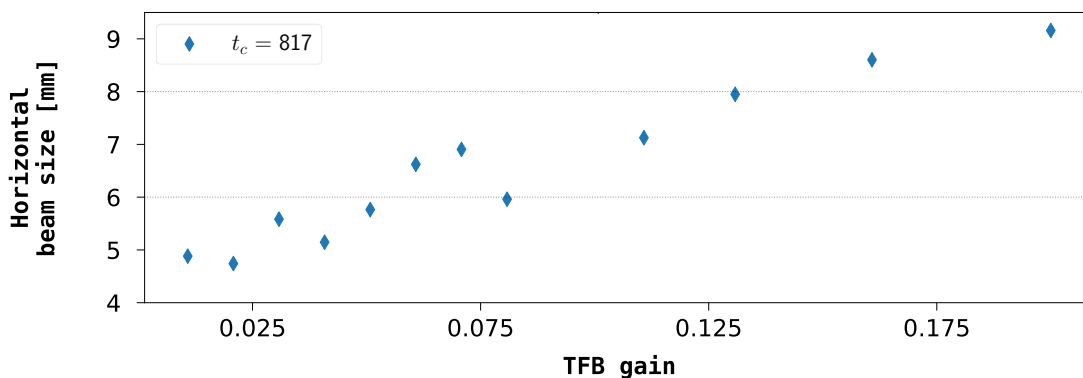


Figure 6.2: Impact of the TFB gain on the horizontal beam size of the core. Plot from [71].

**Tune measurement methodology** During the grid search presented in Section 3.2, the tune was also acquired to find out how reliably it can be used as an observable. Alike the MTE efficiency acquisition, the tune acquisition resulting from the BBQ was averaged over 3 samples. The results are presented in Fig. 6.3. On the left axis, the tune correction setting is shown. The tune acquisition using the BBQ is shown on the right axis. The x-axis represents the different probes that were taken using different settings. The difference in absolute values between both y-axes come about from the acquisition, which measures the absolute value of the tune, and the tune correction setting which sets an offset. As expected, it is visible that both setting and acquisition increase in a proportionate direction.

Especially visible in probe 5 and 6, the results gave an indication that the fluctuations from the acquisition are too high to be a reliable observable.

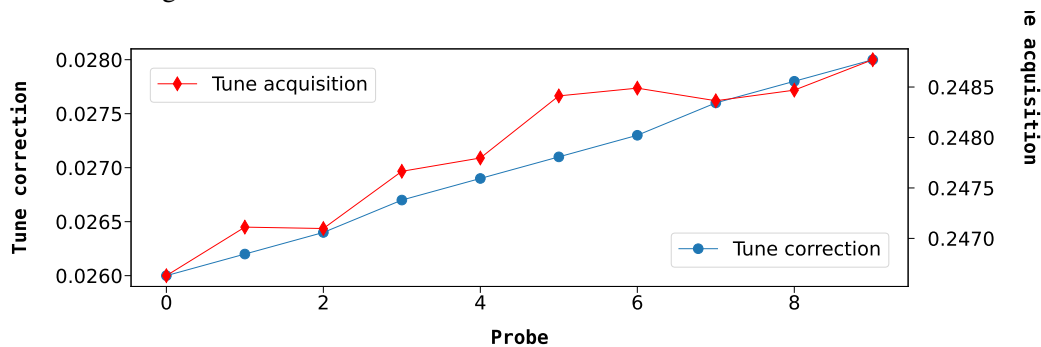


Figure 6.3: Comparing the tune correction settings to the tune acquisition.

This triggered an inquiry to get behind the problem and new settings for the BBQ were then defined in cooperation with device experts. An experiment that compares the tune correction setting to the tune acquisition as in Fig. 6.3 is yet to be done, but the distribution of the fluctuation within the measurements, as seen in Fig 6.4, looks promising. The boxplot shows the distribution of the tune acquisition values. The old methodology, that was active in Fig. 6.3, shows a much larger fluctuation compared to the new method. The sample size  $n$  is annotated in the labels on the left-hand side.

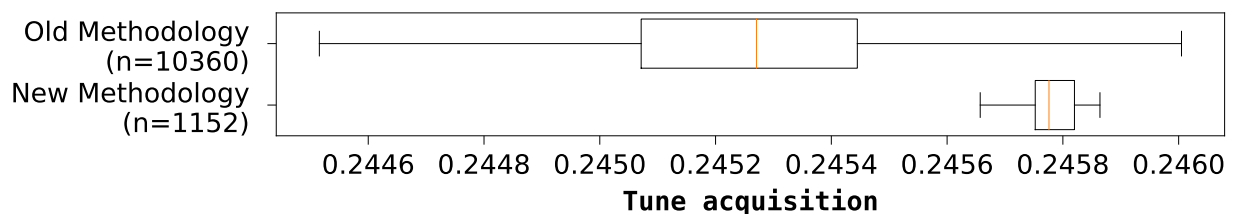
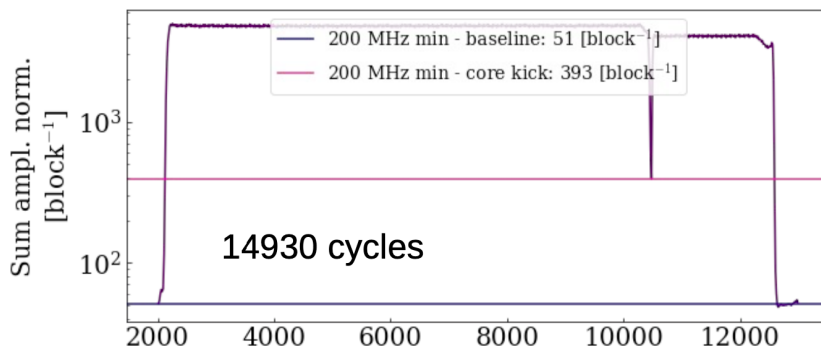


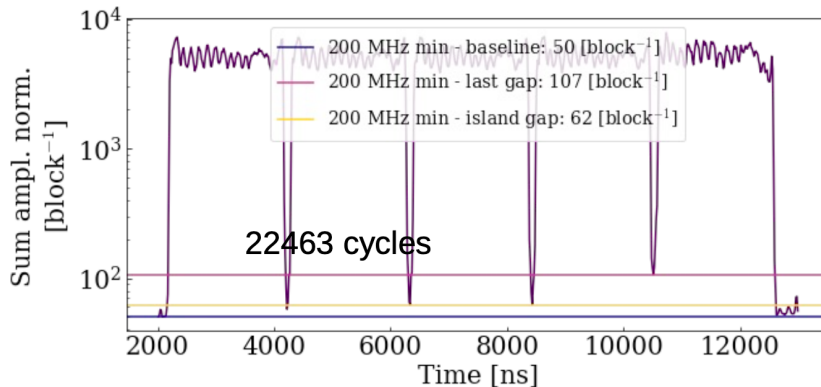
Figure 6.4: Comparing the distribution for different tune acquisition methodologies. The discrepancies visible between the median values are assumed to be caused by a change in intensity on the days that are considered [77]. It was made sure that the distinct data sets themselves have no change in intensity.

**Improved calculation of the MTE efficiency** The changes induced by the BB upgrade are not limited to their primary goal, which is to reduce the beam losses [79]. As the individual beamlets are now separated by a barrier, as visible by the interruptions of the waveform in Fig. 6.5b, the new extraction method will make more accurate MTE efficiency calculations possible by enabling discrimination of the individual islands [80].

The impact of the BB upgrade on the spill waveform is presented in Fig. 6.5. Both graphs show an averaged intensity of the samples from the oscilloscope that is recording the intensity of the transient beam. The upper graph shows the established MTE extraction that was used for the majority of this work. The bottom graph shows the spill when using the BB: the extraction of the individual islands is separated, which is reflected by the visible dips every 2100 ns. The last dip, which is the only one visible in the upper graph, is the separator between the islands and the core of the MTE beam, it reaches a significantly lowered intensity. This distinct separation between the individual islands will allow to determine the MTE efficiency more precisely than before which brings the potential to improve the observable that enters the cost function of the employed algorithms [78].



(a) Standard (Non-BB) extraction method.



(b) BB extraction method.

Figure 6.5: Average spill recorded with BB and non-BB extraction techniques. The plot is taken from [78].

### 6.3 Future implementation

Finally, it is time to discuss the possibility of a future implementation of this algorithm to achieve an operational state. The experiments have demonstrated the potential increase in efficiency that could result from this work. The benefits are two-fold: this method requires less resources from operators as fewer manual interventions will be necessary. Additionally, the performance will be ameliorated compared to the status quo.

Generally, two topics have to be enquired before being able to finish the implementation:

- The obstacles from the BB changes, seen in Section 6.1, will have to be overcome.

As the MTE efficiency is the key figure of merit for this process, this problem will have to be overcome regardless of the outcome of this work. Subsequently, the resources invested in this problem will be coupled to the high priority of this matter which should result in a swift accomplishment after the end of the current YETS.

- Handling of external perturbations.

More experiments towards specific SC configurations will follow the findings in Section 5.2. In combination, the results from the new tune acquisition methodology from Section 6.2 will be evaluated again and hopefully become a reliable indicator to predict the splitting performance.

Supplementary, a safeguard will be implemented whenever the external perturbations become prevalent. This will pause the algorithm and give feedback to the operators on shift which can then decide on further actions based on their experience. As *ES* has shown to recover swiftly after the external factors are removed, this feature should reduce the time required for manual intervention while maintaining the performance benefit.

Following the newly gained insight, the changes will be incorporated into a lightweight GUI application which includes the primary observables for the SFTPRO beam.

**A**

**— APPENDIX —**

### A.1 Correlation with MRP

The mean radial position (MRP) is the averaged position of the beam as measured by the 43 beam position monitors (BPMs) along the accelerator [10]. The physical location within the vacuum chamber is directly linked to the anticipated splitting performance.

As the MRP is logged at a sampling interval of 1 KHz between the injection and ejection of the beam, the correlation between the MRP and the MTE efficiency was inspected at different cycle times. The results of the three highest and lowest correlations are shown in Fig. A.1.

While the relatively strong correlation between the MRPs themselves at different cycle times is expected, the row of particular interest is the row showing the correlation with the MTE efficiency. Unfortunately, the weak correlations prove that the MRP is not suited to deduce additional information about the quality of the splitting.

The data that has been used in this analysis contains every single sample that was recorded using the *LSA* cycle from the MD that is associated to this work. The data has then been smoothed by a rolling mean to soften the fluctuation. It has purposely not been filtered to examine its meaningfulness as an additional observable. Unfortunately, both the correlation presented during this work as well as the correlation considering purely good quality splitting processes have proven to be unsuitable for potential auxiliary usage.

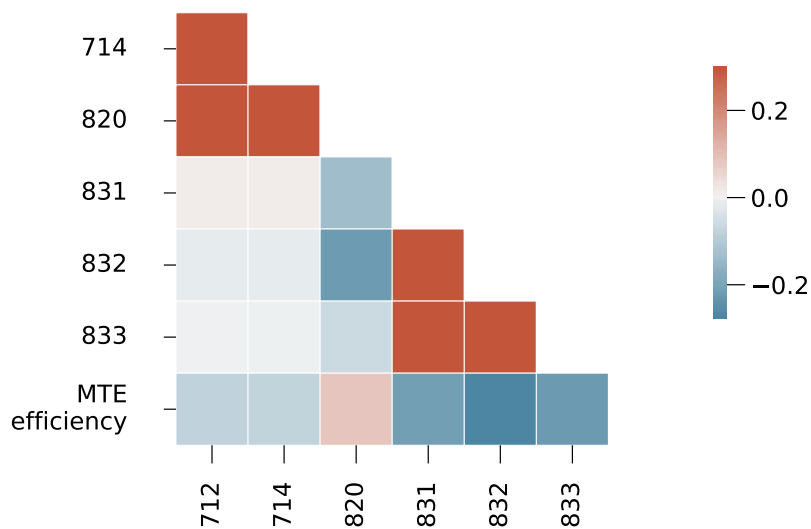


Figure A.1: Correlation matrix between the MTE efficiency and the MRP at different cycle times.

## A.2 – PS magnet layout

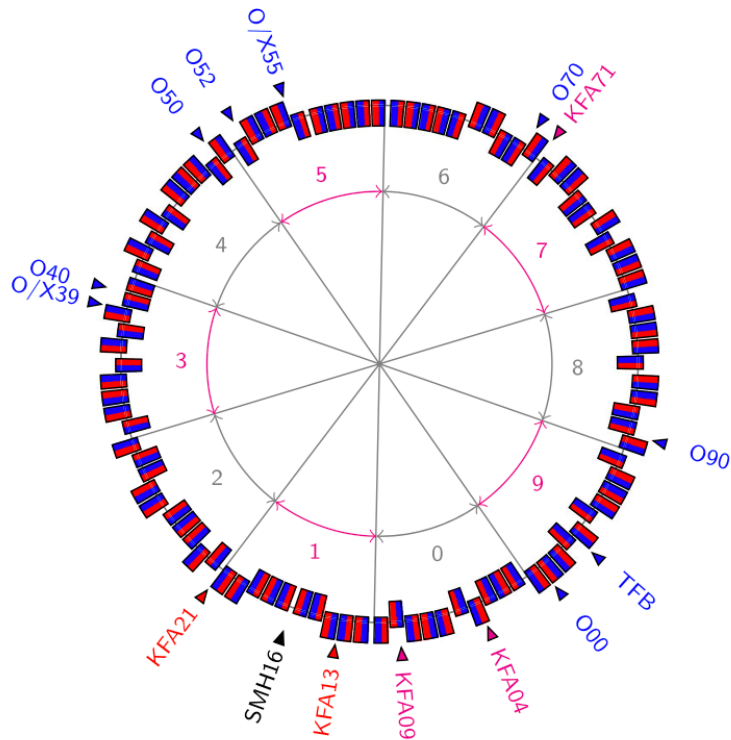


FIG. 1. Layout of the PS ring including the combined-function main magnets (red and blue rectangles for the focusing and defocusing parts, respectively) and the location of the key elements for MTE. The ten different sectors of the PS are indicated by the numbers and the radial offset between the rectangles accounts for the four different magnet types

- Source: [27].
- Additional information: [5].
- X: Sextupole.
- O: Octupole.
- KFA: Kicker Fast. Kicker magnet used for extraction.
- SMH: Septum Magnet Horizontal. Used for extraction.



### A.3 – GeOFF user interface

View Info

CPS 2023-01-20 13:12:51

372

GeOFF v0.7.0 (LSA PS, NO SET)

1 SFTPRO1 | MTE 22

Machine: PS

**TGM User**    **LSA Context**

```

EAST2    EAST_T9_22
SFTPRO1    MTE 22
ZERO    ~zero~
AD    ADO_2000_22
EAST1    EAST_N_22
LHC4    EAST_T9_21
EAST4    IEAST_Pb_1GeVu_22
ION3    ILHC#1b_Pb
ION2    ILHC#1b_Pb80+
ION1    ILHC100#4b_Pb
LHCIND1    LHC#1b_AWAKE
LHCIND2    LHC#1b_INDIV_22
LHCPILOT    LHC#1b_PILOT_22
LHC5    LHC25#12b_3eVs_22
LHC3    LHC25#48b_BCMS_22
LHC1    LHC25#56b_8b4e_22
LHC2    LHC25#72b_3eVs_22
TOF    TOF_22
        
```

⌵ Showing: OPERATIONAL

Num. Optim...    Train RL...    Run R...

**Environment**

AutomatedDriftCorrectionForMTE-v0

Configure

Show constraints

**Algorithm**

Extremum Seeking

Configure

Start    Stop    Reset

Actors

Objective and Constraints

Actors

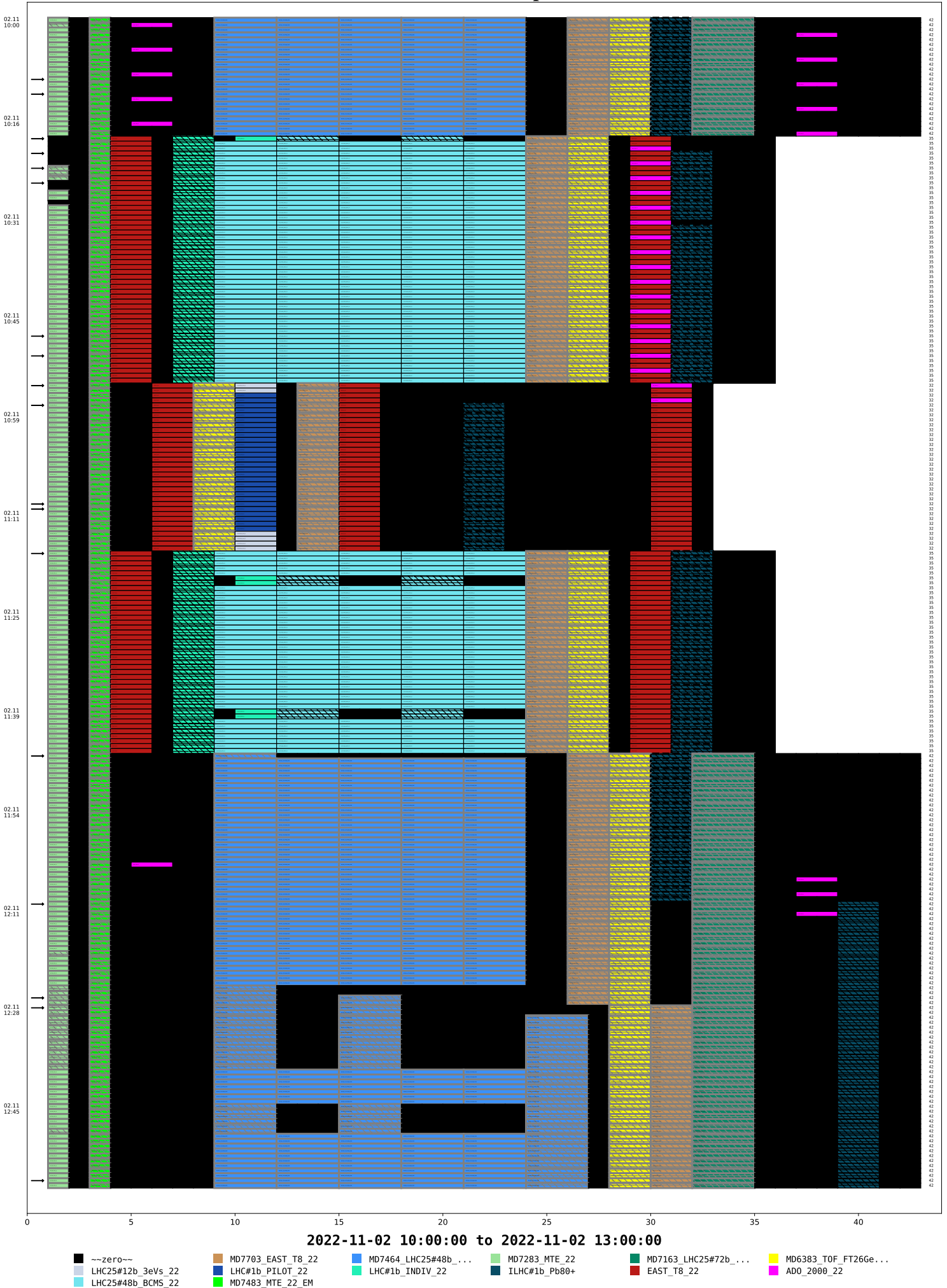
Objective and Constraints

Log Console

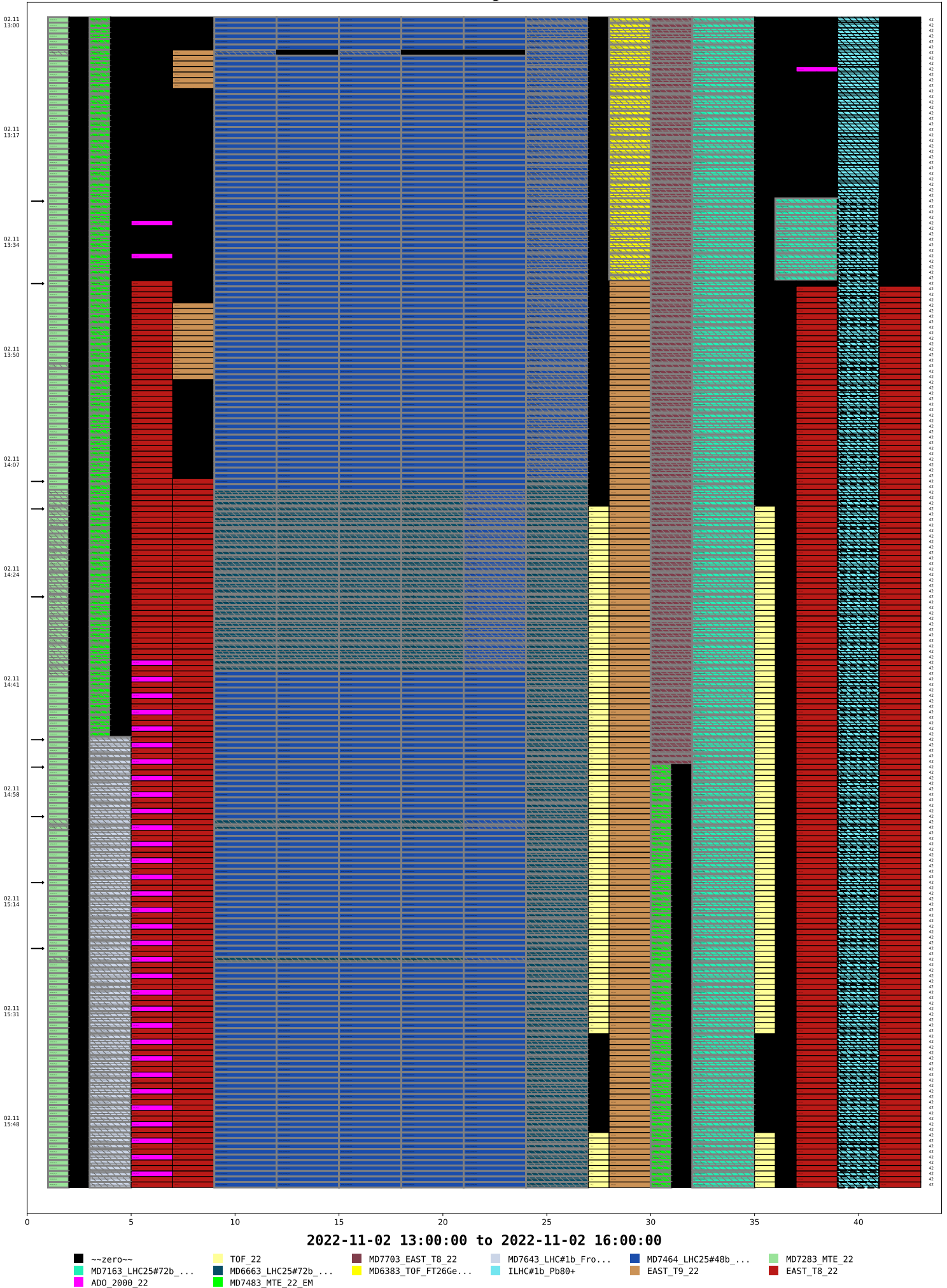
```

2023-01-20 13:12:17,664 - acc_app_optimisation.job_control.single_objective.jobs - INFO - start optimization of AutomatedDriftCorrectionForMTE-v0 using ExtremumSeeking
2023-01-20 13:12:17,933 - pyjapc - WARNING - PA.TFB-DSPU-H/BlowupCtrl#excDDBS1harmonic would be set to:
(double:1) -> 6.250299930657251
2023-01-20 13:12:17,934 - pyjapc - WARNING - PA.TFB-DSPU-H/BlowupCtrl#excDDBS1gain would be set to:
(double:1) -> 0.2199975550174713
2023-01-20 13:12:17,947 - pyjapc - WARNING - PSBEAM/OX LEO would be set to:
(DiscreteFunction:1) -> 0.0 => 0.0; 2.0 => 0.0; 3.0 => 0.0; 4.0 => 0.0; 5.0 => 0.0; 6.0 => 0.0; 7.0 => 0.0; 8.0 => 0.0; 9.0 => 0.0; ... 317 points more
2023-01-20 13:12:24,514 - stderr - INFO - 2023-01-20 13:12:24,514 - [WARNING ] - Atoms.atoms.automated_drift_correction.DetectBeamProblems.DetectBeamProblems.beam_is_available:57 - Beam is not available
this cycle! Beam is available: False. Intensity right after Injection: 0.1.
2023-01-20 13:12:24,517 - stderr - INFO - 2023-01-20 13:12:24,517 - [WARNING ] - Atoms.main.main._compute_single_objective:256 - Problem with Beam availability
2023-01-20 13:12:24,517 - stderr - INFO - 2023-01-20 13:12:24,517 - [WARNING ] - Atoms.main.main._compute_single_objective:256 - Problem with Beam availability
        
```

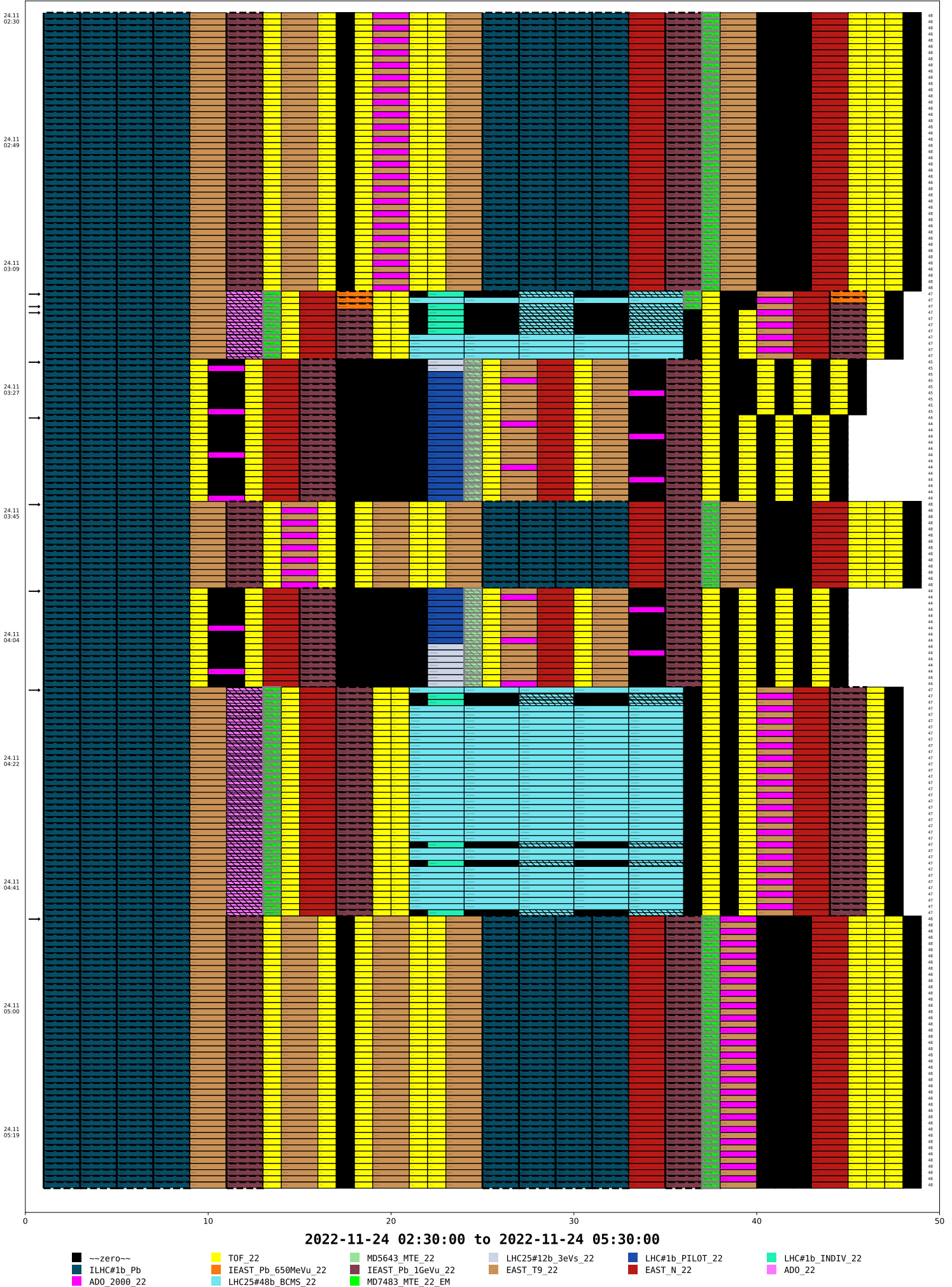
# A.4 - SST example 1



# SST example 2



# SST example 3



---

## B Bibliography

1. Feb. 3, 2023. <https://home.cern/about/who-we-are/our-mission>.
2. Jan. 20, 2023. <https://home.cern/about/who-we-are/our-history>.
3. Brice, M. PS facility - view of the magnets in the Proton Synchrotron. General Photo. <https://cds.cern.ch/record/1748105> (2014).
4. Feb. 3, 2023. <https://www.home.cern/science/accelerators/accelerator-complex>.
5. Gilardoni, S. & Manglunki, D. *Fifty years of the CERN Proton Synchrotron: Volume 1* <https://cds.cern.ch/record/1359959> (CERN, Geneva, 2011).
6. Lee, S. Y. *Accelerator Physics* (World Scientific, Aug. 2021).
7. Feb. 2, 2023. <https://home.cern/science/experiments>.
8. Feb. 3, 2023. <https://www.home.cern/science/accelerators/proton-synchrotron>.
9. Baird, S. Accelerators for Pedestrians. *CERN-Internal*, 1–155 (Jan. 2007).
10. Huschauer, A. Private Communication. 2022.
11. Edwards, D. A. & Syphers, M. J. *An Introduction to the Physics of High Energy Accelerators* ISBN: 0471551635; 9780471551638 (Wiley, Jan. 1993).
12. Forck, P. *Beam Instrumentation & Diagnostics Part 1* in *CERN Accelerator School* (Sept. 2021), 1–74.
13. Steerenberg, R. *Basics of Accelerator Physics and Technology: Basic Mathematics and Units* in (May 4, 2021).
14. Steerenberg, R. & Cotte, D. *PS Beam Spot Sizes For The Design Of New Internal Beam Dumps* tech. rep. (CERN EDMS). <https://edms.cern.ch/document/1612293>.
15. Nolte, D. D. *Introduction to Modern Dynamics: Chaos, Networks, Space and Time* ISBN: 0199657033; 9780199657032 (Oxford University Press, 2015).
16. Hillert, W. *Transverse Linear Beam Dynamics* in *CERN Accelerator School* (Sept. 2021), 1–119.



- 
17. Russenschuck, S. *Field computation for accelerator magnets: analytical and numerical methods for electromagnetic design and optimization* (John Wiley & Sons, 2011).
  18. Damerou, H. *RF Systems* in *CERN Accelerator School* (Oct. 2021), 1–123.
  19. Gasior, M. & Jones, R. *The principle and first results of betatron tune measurement by direct diode detection* tech. rep. revised version submitted on 2005-09-16 09:23:15 (CERN, Geneva, 2005).  
<https://cds.cern.ch/record/883298>.
  20. Jan. 17, 2023. <https://home.cern/science/accelerators/linear-accelerator-4>.
  21. Ordan, J. M. Life in CCC September 2017. General Photo. <https://cds.cern.ch/record/2283167> (2017).
  22. Lopienska, E. The CERN accelerator complex, layout in 2022. Complexe des accélérateurs du CERN en janvier 2022. General Photo. <https://cds.cern.ch/record/2800984> (2022).
  23. Feb. 3, 2023. <https://section-mpc.web.cern.ch/content/tt2>.
  24. Banerjee, D. *et al.* The North Experimental Area at the Cern Super Proton Synchrotron. Dedicated to Giorgio Brianti on the 50th anniversary of his founding the SPS Experimental Areas Group of CERN-Lab II and hence initiating the present Enterprise. <https://cds.cern.ch/record/2774716> (2021).
  25. Cave, S. C. *et al.* Advancing the CERN proton synchrotron multiturn extraction towards the high-intensity proton beams frontier. *Physical Review Accelerators and Beams* **22**, 104002 (Oct. 2019).
  26. Hyde, A. Beams Department Newsletter (December 2015). *CERN-Internal*, 1–17 (Dec. 2015).
  27. Huschauer, A. *et al.* Transverse beam splitting made operational. *Physical Review Accelerators and Beams*, 1–15 (June 2017).
  28. Kain, V. & Madysa, N. *CERNML-COI* CERN, Dec. 20, 2022. <https://gitlab.cern.ch/be-op-ml-optimization/cernml-coi/>.
  29. Brockman, G. *et al.* *OpenAI Gym* 2016. eprint: arXiv:1606.01540.
  30. Beazley, D. & Jones, B. K. *Python Cookbook* (O'Reilly, May 2013).

- 
31. Madysa, N. *GeOFF: Generic Optimization Framework and Frontend* in *CERN Internal Events* (July 2022), 1–68. <https://indico.cern.ch/event/1175862/attachments/2474141/4245177/Madysa%20GeOFF%20BE%20Seminar%202022-07-01.pdf>.
  32. Sinkarenko, I. "Accelerating Python" *PyQt widget library* CERN, Dec. 20, 2022. <https://gitlab.cern.ch/acc-co/accsoft/gui/accsoft-gui-pyqt-widgets>.
  33. Kostro, K. The controls middleware (CMW) at CERN status and usage. *ICALEPS*, 1–5 (Nov. 2003).
  34. Baggiolini, V., Mestre, L., Roux, E., Kruk, G. & Gorbonosov, R. *JAPC - the Java API for Parameter Control* in *ICALEPCS 2005* (Oct. 2005), 1–20.
  35. CERN BE-CSS Group. *PyJapc* CERN, Dec. 20, 2022. <https://gitlab.cern.ch/scripting-tools/pyjapc>.
  36. Feb. 3, 2023. <https://www.python.org/>.
  37. Kruk, G., Deghaye, S., Lamont, M., Misiowiec, M. & Sliwinski, W. LHC Software Architecture [LSA] – Evolution Toward LHC Beam Commissioning. *ICALEPS*, 1–3 (Jan. 2008).
  38. Roderick, C. & Billen, R. *The LSA Database to Drive the Accelerator Settings* tech. rep. (CERN, Geneva, 2009). <https://cds.cern.ch/record/1215575>.
  39. Wozniak, J. & Roderick, C. NXCALS - Architecture and Challenges of the NeXt CERN Accelerator Logging Service. *JACoW*, 1–5 (Oct. 2020).
  40. Dec. 21, 2022. <https://hadoop.apache.org/>.
  41. Dec. 21, 2022. <https://spark.apache.org/>.
  42. Dec. 21, 2022. <https://spark.apache.org/docs/latest/api/python/index.html>.
  43. Raschka, S. & Mirjalili, V. *Python Machine Learning* (Packt, Dec. 2019).
  44. Powell, M. J. D. in *Advances in optimization and numerical analysis* 51–67 (Springer, 1994).
  45. Larson, R. & Edwards, B. *Calculus* 11th (CENGAGE Learning, Dec. 2017).
  46. Soritz, S., Moser, D. & Gruber-Wölfler, H. Comparison of Derivative-Free Algorithms for their Applicability in Self-Optimization of Chemical Processes. *Chemistry-Methods* **2** (2022).

- 
47. Powell, M. J. D. The BOBYQA algorithm for bound constrained optimization without derivatives M.J.D. Powell. *DAMTP*, 1–39 (Aug. 2009).
  48. Stewart, J. *Calculus* 8th (CENGAGE Learning, Jan. 2016).
  49. Virtanen, P. *et al.* SciPy 1.0: Fundamental Algorithms for Scientific Computing in Python. *Nature Methods* **17**, 261–272 (2020).
  50. Cartis, C., Fiala, J., Marteau, B. & Roberts, L. *Improving the Flexibility and Robustness of Model-Based Derivative-Free Optimization Solvers* 2018. <https://arxiv.org/abs/1804.00154>.
  51. Dec. 23, 2022. <https://numericalalgorithmsgroup.github.io/pybobyqa/build/html/userguide.html#optional-arguments>.
  52. Boyd, S., Boyd, S. P. & Vandenberghe, L. *Convex optimization* (Cambridge university press, 2004).
  53. Brunton, S. L. & Kutz, J. N. *Data Driven Science & Engineering* (Cambridge University Press, Apr. 2018).
  54. Ariyur, K. B. & Krstic, M. *Real-Time Optimization by Extremum-Seeking Control* (Wiley-Interscience, June 2004).
  55. Scheinker, A. & Scheinker, D. Extremum seeking for optimal control problems with unknown time-varying systems and unknown objective functions. *Wiley*, 1–19 (Jan. 2020).
  56. Leon, F. P. *Messtechnik* 10th ed. (Springer, Oct. 2015).
  57. Scheinker, A. & Scheinker, D. Bounded extremum seeking with discontinuous dithers. *Automatica* **69**, 250–257 (2016).
  58. Higham, N. J. *Accuracy and stability of numerical algorithms* 1st ed. (Society for Industrial and Applied Mathematics, 1996).
  59. Uden, C. *Injectors Performance Panel: Mini workshop on Efficiency and Automation* Sept. 30, 2022.
  60. Uden, C. Private Communication. 2022.
  61. Kain, V. Private Communication. 2022.
  62. Madysa, N. Private Communication. 2022.
  63. Schenk, M. Private Communication. 2022.
  64. Hostettler, M. Private Communication. 2022.



- 
65. Dec. 19, 2022. [https://www.desy.de/about\\_desy/desy/index\\_eng.html](https://www.desy.de/about_desy/desy/index_eng.html).
  66. Eichler, A., Stein, O. & Kaiser, J. CERN ML Coffee: Reinforcement Learning for Accelerator Optimization and Control. [https://indico.cern.ch/event/1132399/contributions/4751841/attachments/2398209/4100854/20220225\\_DESY\\_CERN\\_ML\\_Coffee\\_new.pdf](https://indico.cern.ch/event/1132399/contributions/4751841/attachments/2398209/4100854/20220225_DESY_CERN_ML_Coffee_new.pdf) (Feb. 2022).
  67. Nonglaton, J.-M. Private Communication. 2022.
  68. Wu, Y. Private Communication. 2022.
  69. Delrieux, M. Private Communication. 2022.
  70. Gramazio, C. C., Laidlaw, D. H. & Schloss, K. B. Colorgorical: creating discriminable and preferable color palettes for information visualization. *IEEE Transactions on Visualization and Computer Graphics* (2017).
  71. Coly, M. Private Communication. 2022.
  72. Mais, H. *et al.* *Cern Accelerator School Vol. 2* (Jan. 1994).
  73. Forck, P. *Beam Instrumentation & Diagnostics Part 2* in *CERN Accelerator School* (Sept. 2021), 1–69.
  74. Damerau, H. *et al.* *LHC Injectors Upgrade, Technical Design Report* <https://cds.cern.ch/record/1976692> (2014).
  75. Sandberg, H. *BGI studies and outlook* in *CERN Internal Events* (Jan. 2023). <https://indico.cern.ch/event/1239885/contributions/5229034/attachments/2584446/4458680/2023-01-31-%20-%20Injectors%20Performance%20Panel%20MD%20days%20-%20BGI%20studies%20and%20outlook.pdf>.
  76. Levasseur, S. *et al.* Development of a rest gas ionisation profile monitor for the CERN Proton Synchrotron based on a Timepix3 pixel detector. *Journal of Instrumentation* **12**, C02050. <https://dx.doi.org/10.1088/1748-0221/12/02/C02050> (Feb. 2017).
  77. Jan. 14, 2023. <https://bpt.web.cern.ch/ps/MTE/2022/>.
  78. Vadai, M. Updates on synchronised PS-SPS transfer with barrier buckets. <https://zenodo.org/record/7334582> (2022).

- 
79. Vadai, M. Beam Manipulations With Barrier Buckets In The CERN PS. *IPAC*, 1–4 (Sept. 2019).
80. Vadai, M. Private Communication. 2022.

## C List of figures

1.1	The <i>Proton Synchrotron</i> . . . . .	14
1.2	Exemplary drift to demonstrate the problem . . . . .	15
1.3	Distribution of beams used for physics production in 2022 . . . . .	16
2.1	Coordinate system within an accelerator ring . . . . .	18
2.2	Transverse emittance in phase space . . . . .	19
2.3	Demonstrating the idea of an RF cavity . . . . .	21
2.4	Motion of a ball in a half-round gutter . . . . .	22
2.5	A typical day in the <i>CCC</i> . . . . .	23
2.6	Visualisation of a supercycle . . . . .	24
2.7	Overview of the <i>CERN</i> accelerator complex . . . . .	26
2.8	Simulation of the beam before and after the splitting process . . . . .	27
2.9	Example of a good and a bad spill . . . . .	28
2.10	Timeline of the MTE splitting . . . . .	29
2.11	Flowchart of the technical frameworks and interfaces . . . . .	32
2.12	Standard framework for a closed-loop controller . . . . .	35
2.13	Comparison of the effects of the <i>ES</i> gain hyperparameter . . . . .	36
3.1	First successful MD slot in this project . . . . .	38
3.2	Problems with <i>ES</i> at the start of the project . . . . .	38
3.3	Distribution of MTE efficiency before the start of this work . . . . .	39
3.4	Grid search of the primary parameters used to control the MTE efficiency . . . . .	40
3.5	Impact of different moving average window sizes . . . . .	40
3.6	<i>COBYLA</i> example episode 1 . . . . .	41
3.7	<i>COBYLA</i> example episode 2 . . . . .	42
3.8	<i>COBYLA</i> example episode 3 . . . . .	42
4.1	Dependency of $C_{\text{Core}}$ on $n_{\text{MTE}}$ and $w_f$ . . . . .	45

---

4.2	Section 4.1 – <i>BOBYQA</i> example episode 1 . . . . .	46
4.3	Section 4.1 – <i>BOBYQA</i> example episode 2 . . . . .	46
4.4	29.10 – 31.10: MTE efficiency evolution influenced by <i>ES</i> over the course of the weekend	47
4.5	Dependency of the cost function on the TFB gain setting and chosen parameter $b$ . . . . .	48
4.6	Section 4.2 – <i>BOBYQA</i> example episode 1 . . . . .	49
4.7	Section 4.2 – <i>BOBYQA</i> example episode 2 . . . . .	49
4.8	31.10: MTE efficiency evolution influenced by <i>ES</i> over the course of the night . . . . .	50
4.9	Developing a metric to quantify the spill quality . . . . .	51
4.10	Comparing the waveform of the spill before and after <i>BOBYQA</i> . . . . .	52
4.11	03.11: MTE efficiency evolution influenced by <i>ES</i> over the course of the night . . . . .	53
4.12	24.11: MTE efficiency evolution influenced by <i>ES</i> over the course of the night . . . . .	54
5.1	External perturbation causing a significant drift . . . . .	56
5.2	Example of the <i>ES</i> behaving unexpectedly under the influence of external perturbations . .	57
5.3	Evidence about the SC dependency of the MTE splitting . . . . .	58
5.4	Extract of an <i>SST</i> page . . . . .	59
5.5	MTE efficiency in dependency of the preceding cycles . . . . .	61
5.6	Distribution of the MTE efficiency of every single SFTPRO MD sample . . . . .	62
5.7	Comparison of operational and MD MTE efficiency distributions . . . . .	63
6.1	Grid search after the barrier bucket upgrades for the SFTPRO cycle . . . . .	65
6.2	Impact of the TFB gain on the horizontal beam size of the core . . . . .	66
6.3	Comparing the tune correction settings to the tune acquisition . . . . .	67
6.4	Comparing the distribution for different tune acquisition methodologies . . . . .	67
6.5	Average spill recorded with BB and non–BB extraction techniques . . . . .	68
A.1	Correlation matrix between the MTE efficiency and the MRP at different cycle times . . .	71

---

## D Acronyms

### List of Acronyms

$t_c$  cycle time. 24, 29

**BOBYQA** *Bound Optimization BY Quadratic Approximation*. 33, 34, 39, 45, 46, 48, 49, 52, 62, 65, 83

**CCC** *CERN Control Centre*. 23, 31, 82

**CERN** *European Organization for Nuclear Research*. 13, 14, 16, 18, 23, 26, 27, 30–33, 82

**CMW** *Controls Middleware*. 31

**COBYLA** *Constrained Optimization BY Linear Approximation*. 33, 34, 39, 41, 42, 62, 82

**COI** *Common Optimization Interface*. 30, 33

**ES** *Extremum Seeking*. 35, 36, 38, 39, 43, 44, 47, 50, 52–54, 56, 57, 61, 63, 65, 69, 82, 83

**FFT** *Fast Fourier Transform*. 22

**GeOFF** *Generic Optimization Frontend and Framework*. 30, 31

**JAPC** *Java API for Parameter Control*. 31, 43

**LHC** *Large Hadron Collider*. 14, 23, 24, 31, 58

**LIU** *LHC injectors upgrade*. 23, 66

**LSA** *LHC Software Architecture*. 24, 31, 43, 61, 71

**NA** *North Area*. 26

**NXCALS** *Next CERN Accelerator Logging Service*. 32

**PSB** *Proton Synchrotron Booster*. 23, 26

**PS** *Proton Synchrotron*. 14, 19–27, 32, 35, 36, 51, 56, 65, 66, 82

**SPS** *Super Proton Synchrotron*. 14, 23, 24, 26

**SST** *Supercycle State Tracker*. 54, 59, 61, 83

**AC** alternating current. 21

**API** application programming interface. 31

**BB** barrier bucket. 65, 68, 69

**BBQ** base band tune. 22, 67

**BCT** beam current transformer. 19

**BGI** beam gas ionisation. 66

**BP** basic period. 24, 43, 59, 60

**BPM** beam position monitor. 71

**EDA** exploratory data analysis. 32

**GUI** graphical user interface. 30, 31, 69

**KISS** keep it short and simple. 39

**LS** long shutdown. 23

**MD** machine development. 24, 26, 27, 29, 32, 56, 60–63, 71, 83

**MRP** mean radial position. 71

**MTE** multi–turn extraction. 27, 28, 34, 38–41, 45, 48, 50, 52, 54–56, 58, 61–63, 65, 67–69, 71

**RF** radiofrequency. 19, 21, 32

**SC** supercycle. 24, 25, 35, 43, 47, 54, 56, 58–62, 69

**SFTPRO** SPS fixed target protons. 27, 29, 35, 43, 58, 61, 63, 66, 69

**TFB** transverse feedback. 29, 39, 45, 48, 50, 66

**YETS** year–end technical stop. 23, 54, 61, 69

